american physiological society

JNP JOURNAL OF NEUROPHYSIOLOGY

J Neurophysiol 130: 751–767, 2023.
First published August 23, 2023; doi:10.1152/jn.00474.2022

RESEARCH ARTICLE

Sensory Processing

Enhancement of phase-locking in rodents. II. An axonal recording study in chinchilla

Liting Wei, Eric Verschooten, and Philip X. Joris
Laboratory of Auditory Neurophysiology, KU Leuven, Leuven, Belgium

Abstract

The trapezoid body (TB) contains axons of neurons residing in the anteroventral cochlear nucleus (AVCN) that provide excitatory and inhibitory inputs to the main monaural and binaural nuclei in the superior olivary complex (SOC). To understand the monaural and binaural response properties of neurons in the medial and lateral superior olive (MSO and LSO), it is important to characterize the temporal firing properties of these inputs. Because of its exceptional low-frequency hearing, the chinchilla (*Chinchilla lanigera*) is one of the widely used small animal models for studies of hearing. However, the characterization of the output of its ventral cochlear nucleus to the nuclei of the SOC is fragmentary. We obtained responses of TB axons to stimuli typically used in binaural studies and compared these responses to those of auditory nerve (AN) fibers, with a focus on temporal coding. We found enhancement of phase-locking and entrainment, i.e., the ability of a neuron to fire action potentials at a certain stimulus phase for nearly every stimulus period, in TB axons relative to AN fibers. Enhancement in phase-locking and entrainment are quantitatively more modest than in the cat but greater than in the gerbil. As in these species, these phenomena occur not only in low-frequency neurons stimulated at their characteristic frequency but also in neurons tuned to higher frequencies when stimulated with low-frequency tones, to which complex phase-locking behavior with multiple modes of firing per stimulus cycle is frequently observed.

NEW & NOTEWORTHY The sensitivity of neurons to small time differences in sustained sounds to both ears is important for binaural hearing, and this sensitivity is critically dependent on phase-locking in the monaural pathways. Although studies in cat showed a marked improvement in phase-locking from the peripheral to the central auditory nervous system, the evidence in rodents is mixed. Here, we recorded from AN and TB of chinchilla and found temporal enhancement, though more limited than in cat.

chinchilla; peak-splitting; phase-locking; temporal coding; trapezoid body

INTRODUCTION

Accurate neural encoding of temporal sound features is important for spatial hearing and other aspects of perception. One striking manifestation of such encoding is the ability of auditory neurons to code the fine structure of the sound waveform, i.e., its instantaneous pressure fluctuations. The simplest demonstration of this ability is with pure tones: peripheral neurons restrict their firing of action potentials over a limited phase range within the cycles of a pure tone, for frequencies up to several kilohertz (1–3). Such phase-locking is a necessary condition for the creation of neural sensitivity to interaural time differences (ITDs) of low-frequency sounds in the auditory brainstem, which is one of the main cues to localize sounds in the azimuthal plane (4). Sensitivity to ITDs first arises in the superior olivary complex (SOC) (5, 6). The exact cellular mechanisms involved are still controversial but their study has steadily progressed mainly through the use of new techniques in small animal models, particularly the gerbil (7–12).

A limitation of the gerbil model is that, despite having an audiogram that extends to quite low frequencies (13), there appears to be little frequency tuning below ~500 Hz. Threshold tuning curves of auditory nerve (AN) fibers only rarely reveal a characteristic frequency (frequency of lowest threshold, CF) below that limit (14–18), and the same holds for neurons in the anteroventral cochlear nucleus (AVCN) (19) and for fibers in its output tract, the trapezoid body (TB) (20), as well as for binaural neurons in the SOC (11, 21). In contrast, there is extensive psychophysical evidence for bandpass filters tuned to frequencies below 500 Hz in humans (22). Even though human ITD

Correspondence: P. X. Joris (Philip.Joris@kuleuven.be).
Submitted 16 November 2022 / Revised 7 August 2023 / Accepted 15 August 2023

0022-3077/23 Copyright © 2023 the American Physiological Society.

Downloaded from journals.physiology.org/journal/jn (081.164.135.205) on July 13, 2026.

sensitivity to the fine structure of sound waveforms extends up to ~1.3 kHz when studied with pure tones (23), binaural detection data in humans are well-modeled by a low-pass synchronization filter with a corner frequency of only 425 Hz (24) and a "dominance" region centered near 600 Hz (25, 26). In response to broadband sounds, peripheral frequency filtering strongly affects the output of ITD-sensitive neurons (27, 28), and some form of integration across frequency channels is thought to be important in binaural hearing (29). Thus, the absence of frequency tuning in gerbils, over a good part of the frequency range that is important for human binaural hearing, limits its value as a model for human binaural hearing.

The chinchilla is another popular auditory rodent model, with very sensitive hearing extending as low as 100 Hz (30). The auditory periphery of the chinchilla has been rather well-characterized physiologically (31–39) and, unlike the gerbil, the chinchilla has cochlear tuning (rather than just sensitivity) to frequencies as low as ~200 Hz (35, 40). Another, perhaps underappreciated advantage of chinchilla is that the enormous bulla enables easy access to ventral and lateral brainstem structures. We have exploited this anatomy to gain access to axons of brainstem neurons projecting into the SOC or ascending in the lateral lemniscus and found that this approach is an excellent way to study both the inputs and the outputs of the MSO (41). We use the descriptions TB axon and TB fiber interchangeably.

The present study is the second part of a general assessment of monaural components of the ITD circuitry in rodents (gerbil and chinchilla) in the context of studies in our laboratory of binaural sensitivity in these species (11, 41, 42). A striking phenomenon, first observed with pure tones in the cat (43, 44), is an enhancement in phase-locking between AN and AVCN. This enhancement extends to broadband stimuli (45) and is thought to benefit binaural temporal sensitivity (46, 47). For reasons that are not entirely clear, this enhancement in the cat was much more significant in recordings from TB fibers than from AVCN proper. The literature on the properties of phase-locking and entrainment in the AVCN of chinchilla to pure tones is limited (32, 38). Our goal here is to examine phase-locking and entrainment in TB fibers to pure tones, both at CF and off-CF. To better interpret the results, we compare these responses with data obtained in the AN and include a small sample of data from neurons in the medial nucleus of the TB (MNTB).

METHODOLOGY

Adult wild-type chinchilla (*Chinchilla lanigera*) of both sexes, free from middle ear infection and weighing between 200–700 g, were used. The animals were housed in a licensed breeding facility. The animal procedures were in accordance with the European Communities Council Directive (86/609/EEC) and approved by the animal ethics committee of the University of Leuven.

Surgical Preparation

Anesthesia was induced by an intraperitoneal injection of a mixture of ketamine (20 mg/kg) and xylazine (3 mg/kg) and maintained with intramuscular injections of ketamine (8.3 mg/kg) and diazepam (0.42 mg/kg) when the animal showed signs of corneal reflex and/or paw pinch reflex. The animal was placed in a double-walled sound-proof room (Industrial Acoustics Company, Niederkruchten, Germany) in a recumbent position on a heating pad. This pad was feedback-controlled to keep rectal temperature at a target value of 37°C. To limit heat loss, the body of the animal was covered with a paper towel. A head mount was secured with dental cement to the exposed frontal skull. A tracheotomy was routinely performed to avoid airway obstruction during the experiment. The pinna was removed on both sides to allow tight-fitting ear bars to fit in the rim of the bony ear canal. Petroleum jelly was used to seal gaps between ear bars and bulla. The acoustic systems in the right and left ears were calibrated with probe tubes extending slightly inside the bulla opening.

The ventral brainstem was accessed via a transbulla approach. The tympanic bulla on both the left and right sides was opened medially to maintain acoustic symmetry. A small fenestration was carefully made in the "roof" of the bulla to expose the TB on one side. The meningeal layers were carefully removed with a hooked needle to enable smooth penetration of the glass electrode into the TB. During the experiment, the brainstem was kept moist with drops of saline. Access to the AN was via the traditional posterior fossa approach, involving the removal of a small portion of lateral cerebellum and the use of pieces of saline-soaked cotton to retract the brainstem from the bone, thereby exposing the AN.

Acoustic Stimulation and Recording

Acoustic stimuli were delivered through dynamic earphones (Supertweeter, Radio Shack, Fort Worth, TX) connected with tubing to plastic earpieces. Acoustic stimulation and acquisition of signals used custom software, using digital hardware (Tucker-Davis Technologies, system II, Alachua, FL). The transfer function of the closed acoustic system of both sides was derived with the probe tip coupled to an ½ in. (12.7 mm) condenser microphone and conditioning amplifier (Type 2609, Bruel & Kjær, Copenhagen, Denmark). Stimuli were all compensated for this transfer function. Routine methods were used for recording, amplification, and filtering (300–3,000 Hz), and spikes were converted to standard pulses with a custom-built peak-picker and were time-stamped at 1-μs resolution.

Recording

Micropipettes were pulled (Flaming/Brown puller P-87) from borosilicate glass (WPI 1B100F-6) for an impedance of 60–120 MΩ after filling with 2 M KCl. They were mounted in a hydraulic microdrive (Trent Wells, Coulterville, CA) supported by a micromanipulator and advanced into the TB or AN after visually guided placement. The point at which the tip of the micropipette penetrated the brain surface was marked as 0 in depth, estimated based on visual and electrophysiological signs. The microelectrode was then advanced in 1-μm steps until large monopolar action potentials of a single axon were encountered. In some cases, intracellular signals were recorded as the electrode penetrated the axon (signaled by an increase in action potential amplitude and a negative DC shift of several tens of mV). Extracellular and intracellular signals were monitored on an oscilloscope (model DPO 3014, Tektronix). Agar (2%) was poured on the TB or AN

Downloaded from journals.physiology.org/journal/jn (081.164.135.205) on July 13, 2026.

to reduce brainstem pulsations. For extracellular recording of MNTB principal cells, glass micropipettes of lower impedance (5–20 MΩ) were used, obtained by mechanically breaking back the tip of the pipette.

Stimuli

A search stimulus of short-tone bursts varied in logarithmic frequency steps [duration 250 ms, repeated every 300 ms, 60–70 dB sound pressure level (SPL), 200–15,000 Hz] was presented to both ears as the electrode was advanced into the TB until a single axon was isolated, as judged based on spike amplitude and presence of a refractory period. After determination of the excitatory ear, we measured spontaneous rate (SR: estimated over a 15-s interval preceding acoustic stimulation) and CF using a tracking algorithm, and collected responses to several stimuli, as allowed by the recording time. Binaural neurons are not further considered in the analysis. Responses to short-tone bursts (duration 25 ms, repeated every 100 ms, 200 repetitions, raised-cosine ramps of 2.5 ms) were then presented at different SPLs in 5–10 dB steps, covering an SPL range from below threshold to 90 or sometimes 95 dB (nonrandomized, from low to high SPL). At very low frequencies (<500 Hz), duration parameters were doubled (50 ms every 200 ms). Data collection typically started with short tones at the CF (STCF). In some cases, responses to the same STCF stimuli were collected from both ears, to assess interaural attenuation (see RESULTS, Fig. 11). We were particularly interested in assessing phase-locking and, if time allowed, obtained responses to off-CF low-frequency tones (<1 kHz). High-CF TB fibers were studied with low-frequency stimuli if they responded at SPLs not exceeding 90–95 dB. Following use in the literature, we describe these stimuli as being in the "low-frequency tail," even if the tuning curve did not show disjunct tail and tip regions. For comparison, we include data from the AN collected in the context of other studies of our laboratory (48–50). These recordings followed a protocol similar to the TB recordings. It is inherent in these types of axonal recordings, where mechanical stability is a major limitation, that data collection has to be segmented into blocks where only a single stimulus parameter is varied. Within such a block, which we refer to as a "data set," typically all stimulus parameters are fixed (including frequency) and only SPL is varied. Being the basic unit of data collection, we therefore often state not only the number of neurons but also the number of datasets in which an observation was made.

Data Analysis

The description below concerns the responses of TB fibers. For those metrics where a comparison with the AN was of interest, the same analysis was applied to the responses of AN fibers.

The response to STCF was used to construct post-stimulus-time histograms (PSTHs) with 0.1 ms bin width. Neurons were classified according to the widely used scheme based on the shape of the PSTH (51–57), which was examined over a wide range of SPLs. In short, we separate the recordings into six main response types (see also Figs. 1 and 2). Our main interest is in four types that we group as "bushy-type": these include primary-like (PL), primary-like-with-notch (PL_N), phase-locked (PHL), and a small sample of neurons in the medial nucleus of the trapezoid body (MNTB). PL responses are similar to AN responses with an initial peak followed by a monotonic decline in instantaneous rate to a steady-state response and are dominantly associated with spherical bushy cells. PL_N responses show a well-timed onset followed by a "notch" of inactivity of a few milliseconds and are associated with globular bushy cells. Responses of fibers with low CF (<1 kHz) that show phase-locking to the fine structure of the STCF are categorized as PHL. When recorded in the TB, these responses are associated with either spherical or globular bushy cells (57). A small sample of responses from low-CF MNTB neurons with PHL-type PSTH was collected as an indirect indicator of globular bushy cell characteristics. MNTB neurons were identified based on the presence of a prepotential and their monaural responsiveness to contralateral stimuli. Onset (O) responses consist of an onset peak followed by little or no sustained activity. Chopper (CHOP) responses are rhythmic at intervals that are not related to the stimulus period.

The vector strength R (5) was determined from the responses to pure tones as a measure of the strength of phase-locking. R is the Fourier component of the PSTH at the stimulus frequency, normalized to the total number of spikes (3). The vector strength was calculated over an analysis window of 10 ms postonset to the end of the stimulus time window to accommodate response latency and omit the response to stimulus onset. For each fiber, R was calculated at all SPLs for which responses were available and the maximum R value (R_{max}) was determined. The statistical significance of the R values ($P < 0.001$) was evaluated with Rayleigh's test (58). An R_{max} value ≥ 0.9 is called "high-sync," as such values are only very rarely obtained in the chinchilla AN in response to tones at CF (38).

The entrainment index (EI) (43) is a simple metric to quantify how consistent phase-locked responses are in producing an action potential at each cycle of the stimulus: it equals the number of first-order interspike intervals equaling the stimulus period, give or take half a period, divided by the total number of intervals. It is valued from 0 to 1, where 1 indicates that the fiber fires a single spike on every stimulus cycle and 0 indicates that it never fires on two subsequent cycles. EI values were calculated over the same response window as R (10 ms to the end of the stimulus time window) at each sound level, and the maximum value (EI_{max}) was determined. Only responses yielding ≥100 spikes or intervals (accumulated over all stimulus repetitions), within this response window were used for the calculation of R and EI.

Peak latency is defined as the poststimulus time at which the discharge rate reaches 20% of the peak driven rate (= absolute rate − SR) of the PSTH (bin width 0.1 ms with 3-point triangular smoothing) (59). Nonmonotonicity of the rate-level curve is defined as a decrease of at least 30% in spike rate between the spike rate peak and the rate from the highest sound level presented after three-point smoothing (60).

RESULTS

Our main interest was in the phase-locking behavior of bushy-type neurons, which we characterized by responses over a wide range of SPLs for each neuron, in response to

Downloaded from journals.physiology.org/journal/jn (081.164.135.205) on July 13, 2026.

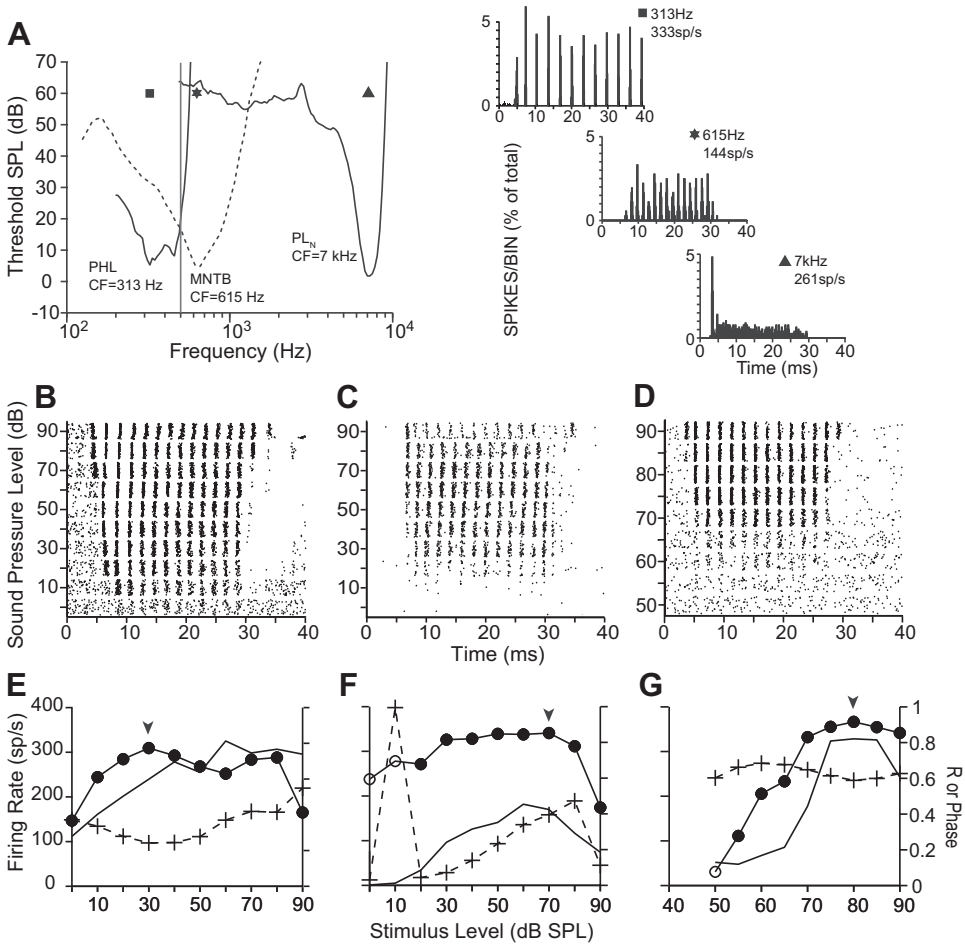


Figure 1. Examples of three bushy-type neurons phase locking to low-frequency tones. *A*: threshold tuning curves; three-point-smoothing was applied. Characteristic frequency (CF) is indicated on graph. Neurons were classified according to the poststimulus-time histogram (PSTH) to tone bursts at CF, of which examples (at 60 dB SPL) are shown on the *right*. Two recordings were from axons in the trapezoid body (TB) (solid lines): these generated a PHL and PL_N response pattern (indicated by a filled square and triangle, respectively). One recording was from a neuron in the medial nucleus of the TB (MNTB) (dotted tuning curve), which also generated a PHL response pattern (indicated by star). *B–D*: raster plots show responses of these three neurons to increasing intensity of a 500-Hz tone burst. Panels are arranged from low to high CF. *E–G*: firing rate (left ordinate) and phase locking (magnitude R and phase in cycles, right ordinate) of the responses to 500 Hz. Solid lines without symbols indicate firing rate; circles indicate R values; plus symbols indicate average phase. Filled circles indicate that the R value is significant by Rayleigh's test. R_{max} for each neuron is highlighted by an arrowhead. PHL, phase-locked; PL_N, primary-like-with-notch; TB, trapezoid body.

short pure-tone bursts at the CF and other frequencies. Vector strength R was calculated for all SPLs and the maximum value R_{max} was used as a summary metric for the ability of neurons to phase-lock to fine-structure. Three examples in Fig. 1 illustrate the procedure. The solid lines in Fig. 1*A* show threshold-tuning curves of two TB fibers. PSTHs obtained to STCF at 60 dB are shown to the right of the tuning curves. The low-CF (313 Hz) fiber was classified as PHL, and the high-CF (7 kHz) fiber as PL_N. The low-CF fiber clearly shows excellent phase-locking (R_{max} = 0.989); the high-CF fiber showed no significant phase-locking at CF at any SPL. Previous labeling studies strongly suggest that these axonal recordings are from bushy-type neurons (57, 61), but there is no certainty, particularly for fibers with the PHL response pattern, which can be generated by many neuron types. The dotted tuning curve and accompanying PSTH are from a neuron with a PHL response where the extracellular spike showed a prepotential. Combined with the monaural, contralateral response, and the recording location, this is a strong indication that this recording was from an MNTB neuron: it also shows excellent phase-locking (R_{max} = 0.911). Responses were also obtained at low frequencies off-CF, e.g., at 500 Hz (Fig. 1*A*, vertical line), for which responses are illustrated by the dot rasters in Fig. 1, *B–D*. Responses are phase-locked for all fibers, showing features documented in previous studies. Phase-locking starts at very low SPL, in the form of a regrouping of spikes (Fig. 1, *B–D*). It shows an orderly pattern across SPL, with moderate and gradual changes in phase. More abrupt changes are visible at high SPL (90 dB) in all three neurons: a drop in firing rate (Fig. 1*G*), a drop in R (Fig. 1, *E* and *F*), and a large change in phase (Fig. 1*F*). The phase-locking can show a pattern of temporal adaptation (Fig. 1, *B* and *D*) where spikes are more tightly distributed for initial than for later stimulus cycles. Finally, although clear phase-locking is present in all three neurons to a 500-Hz off-CF stimulus, R_{max} is highest in the high-CF neuron (Fig. 1, *E–G*, arrowheads indicate R_{max}: respectively 0.77, 0.85, and 0.92). The features outlined in Fig. 1 are very reminiscent of those observed in cat (43, 44, 62), and more specifically suggest that the phenomenon of enhanced phase-locking ("high-sync neurons") in bushy cells also applies to the chinchilla. We examine this with the population analyses in the two following sections, below.

We recorded from 135 single fibers coursing in the TB of 26 chinchillas. They were classified according to their PSTH to the following groups: PL_N (n = 59), PL (n = 21), PHL (n = 45), O (n = 5), and CHOP (n = 5). There was a small number of fibers (n = 6) that did not fit into these categories and they are not further considered in this paper. A small sample (n = 3) of low-CF MNTB neurons is also presented. Representative PSTHs of each response type are illustrated in Fig. 2, *A–L*, with their CF and sustained spike rate. For reference, the TB responses were compared with those of several hundred AN fibers.

Downloaded from journals.physiology.org/journal/jn (081.164.135.205) on July 13, 2026.

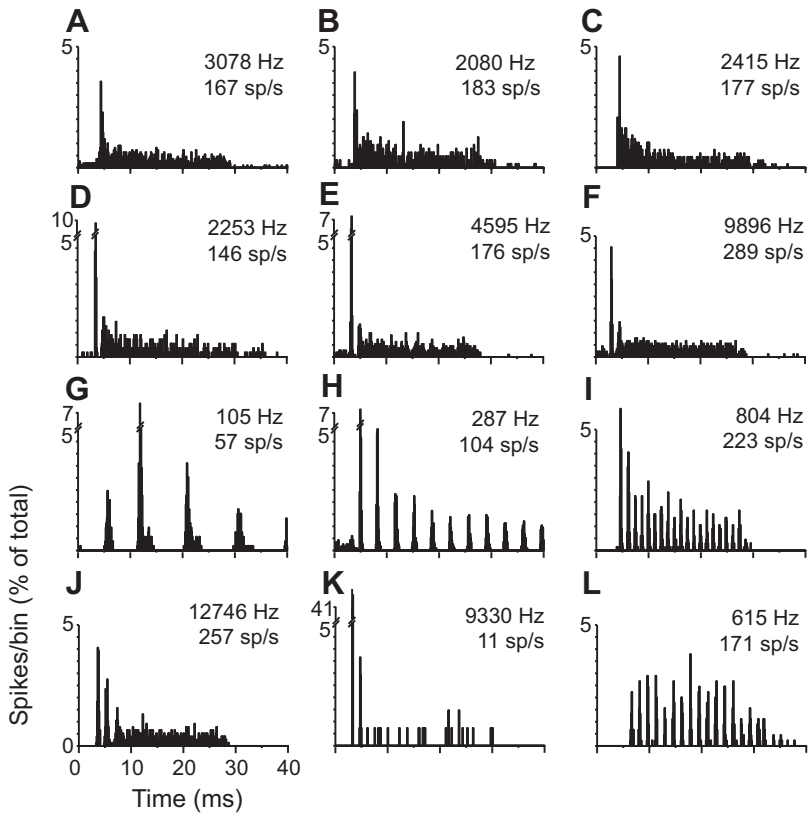


Figure 2. PSTHs of TB fibers (*A*–*K*) and an MNTB neuron (*L*) in response to short tones at the characteristic frequency (CF). The CF and sustained rate, calculated over a 10–25 ms window, are shown above each PSTH. *A*–*C*: examples of primary like (PL) responses at suprathreshold levels of 60, 70, and 75 dB. *D*–*F*: primary-like-with-notch (PL_N) responses at 80, 70, and 80 dB. *G*–*I*: phase-locked (PHL) responses at 80, 85, and 70 dB. *J*–*K*: chopper (CHOP) and onset (O) responses at 80 dB. *L*: PHL response at 80 dB of an MNTB cell (same cell as in Fig. 1). Abscissa and ordinate scales are identical for all panels. Ordinate shows spikes/bin as a percentage of the total number of spikes. Note that in panels with large onset responses (*E*, *H*, and *K*) the *y*-axis is interrupted and extended to accommodate the large peaks. For example, for the PSTH of the O response (*K*), more than 40% of the spikes occurred in a single bin at stimulus onset. MNTB, medial nucleus of the TB; PSTH, post-stimulus-time histograms; TB, trapezoid body.

Synchronization and Entrainment to CF Tones

R_{max} at CF is shown in Fig. 3*A* as a function of CF for the recorded population on an expansive ordinate scale (3). The significance ($P < 0.001$) of phase-locking is indicated by the symbol: a solid symbol for significant and an empty symbol for nonsignificant values. The filling color indicates the SPL range at which R_{max} was obtained (see caption in Fig. 3*A*). An R_{max} trendline is shown (lowess, span 60%, Matlab, solid black line). Due to the low number ($n = 6$) of TB fibers with CF below 200 Hz, the TB trendline is calculated using fibers with significant R_{max} and CF > 200 Hz. The "high-sync" criterion of $R_{max} = 0.9$ is indicated by the horizontal line. The R_{max} values against CF show a low-pass shape, as has been observed in other species (20, 43, 53–55, 63). As CFs increase above 3 kHz, there are an increasing number of nonsignificant R_{max} values. The highest frequency at which significant phase-locking occurred was 3.7 kHz, indicated by the arrowhead in Fig. 3*A*.

To properly assess enhanced phase-locking, a comparison with AN is needed. Figure 3*A* shows two trendlines to summarize AN data: the red line is for our data (individual data are shown in Fig. 5*A*); the dotted line is for data of Recio-Spinoso (38). Compared with the average R_{max} values of around 0.8 for AN fibers with CF < 1 kHz, the TB data showed clear enhancement. All data points for CF < 700 Hz are above the AN trendlines, and about half (16/33) of these TB fibers are classified as "high-sync" with $R_{max} > 0.9$. Note however that most of these 16 data points are rather close to that criterion, unlike the distribution in cat (43), except for three fibers with extremely high values. Comparison of the TB and AN trendlines shows a pattern similar to the cat (44, Fig. 4) and gerbil (21, Fig. 2): at low CFs, R_{max} values tend to be higher in the TB than in the AN, whereas the opposite is the case at higher CFs. The crossover point is somewhat below 1 kHz, as it is in these other species.

It is of interest to examine at which intensities R_{max} tended to occur: this is indicated by the color code, which partitions the intensity range into low (≤40 dB), mid (>40 to <70 dB), and high (≥70 dB) ranges. In particular, at high SPLs, AN fibers can show spiking patterns that strongly deviate from the patterns shown at lower SPLs (see below). It is not the case that R_{max} values were restricted to high intensities. The majority (53/83) of R_{max} values occurred at stimulus levels <70 dB SPL (Fig. 3*A*, blue and black symbols).

In the auditory central nervous system (CNS), timing and firing rate become entangled through the phenomenon of entrainment, i.e., the firing of spikes on (nearly) every stimulus cycle (43, 54). Entrainment increases trial-to-trial consistency, and combined with enhanced phase-locking, benefits binaural temporal comparisons (46, 47). The maximal entrainment index (EI_{max}) of bushy-type TB fibers in response to CF-tones is shown in Fig. 3*B*. Only five low-CF fibers displayed high entrainment ($EI_{max} > 0.9$): they all had CF < 500 Hz. The solid line representing the trend of EI_{max} values for chinchilla (lowess, span 60%, Matlab) is clearly lower than that for the cat (dashed line, lowess, span 25%, calculated for the data of Ref. 43). Thus, only a few of the high-sync responses were accompanied by high entrainment. This limitation in entrainment in chinchilla is also noticeable in the second metric that we examined: maximal

Downloaded from journals.physiology.org/journal/jn (081.164.135.205) on July 13, 2026.

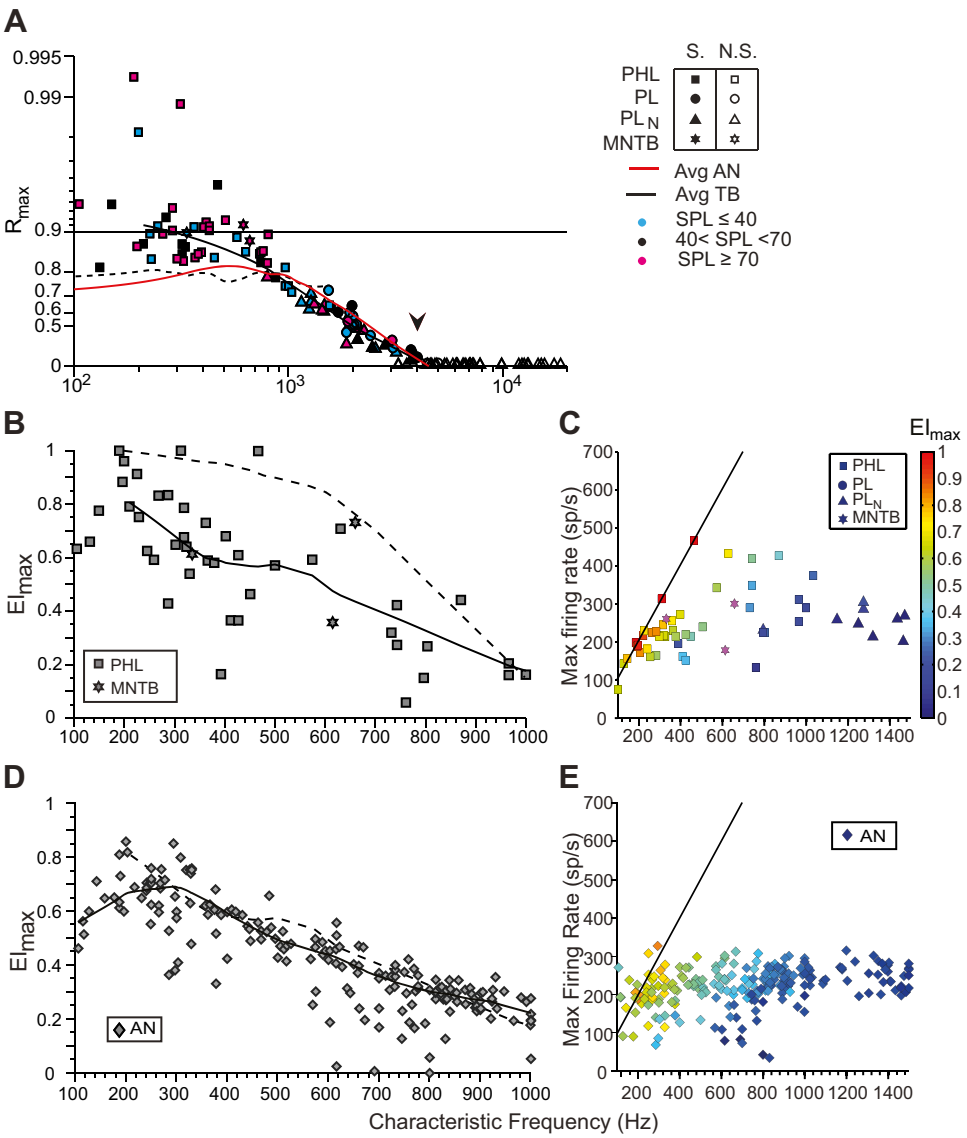


Figure 3. Strength of phase locking and entrainment of different types of TB fibers at CF. *A*: strength of phase-locking in TB fibers, compared with the auditory nerve (AN). R_{max} is graphed against CF. Phase-locking is significant for the filled symbols. The black arrowhead points to the highest CF with significant phase-locking. Color indicates the SPL at which R_{max} was obtained, using the ranges indicated in the *inset*. The red and black solid line are trendlines for AN and TB data, respectively. The TB trendline excludes MNTB data (lowess, span 60%). The primary data for the AN trendline (lowess, span 30%) are shown in Fig. 5*A*. The dashed line is a trendline for the AN data of Recio-Spinoso (38) (lowess, span 25%). The horizontal line at $R_{max} = 0.9$ marks the "high-sync" criterion. Note the expansive scale of the ordinate, obtained by plotting $(1-R_{max})$ on a logarithmic and inverted scale (3). *B* and *C*: entrainment to CF tones in TB fibers. *B*: maximum value of entrainment index (EI_{max}) as a function of CF for the frequency range 100–1,000 Hz. Square and star symbols represent the EI_{max} of neurons with a PHL response ($n = 43$) and of MNTB cells ($n = 3$). Solid and dashed lines are trendlines for TB fibers of chinchilla and cat (43), respectively (lowess, span 60%, datapoints < 200 Hz excluded). *C*: maximum firing rate for bushy-type fibers stimulated at CF. The line in the graph is the unity line and the color indicates the EI_{max}, as indicated by the color bar. Symbols identify different classes. *D* and *E*: entrainment to CF tones in AN fibers. *D*: maximum value of entrainment index (EI_{max}) as a function of CF for chinchilla AN ($n = 463$). Solid and dashed lines are trendlines for chinchilla AN and TB fibers (the latter taken from *B*), respectively. *E*: maximum firing rate of AN fibers. The line in the graph is the identity line and the color indicates EI_{max} (color bar in *C*). CF, characteristic frequency; MNTB, medial nucleus of the TB; PHL, phase-locked; PL, primary-like; PL_N, primary-like-with-notch; SPL, sound pressure level; TB, trapezoid body.

firing rate (Fig. 3*C*). Because perfect entrainment implies the firing of one spike with every cycle, perfectly entrained firing to CF tones implies an increase in firing with CF along the line of equality (Fig. 3*C*, solid line). Indeed, this line sets an upper bound on the firing rates observed, which tended to increase with CF up to ~600 Hz, and responses close to this line show high EI_{max} values ("warm" colors). However, consistent with the EI measurements (Fig. 3*B*), few responses are on the line of equality. A third indication of the limited entrainment in TB fibers is the comparison with AN fibers. Figure 3, *D* and *E*, shows AN population data, using the same metrics as in Fig. 3, *B* and *C*. The trendline of the TB fibers (Fig. 3*B*, solid line) is replotted in Fig. 3*D* as a dashed line: it is tracked rather closely by the trendline for AN fibers (Fig. 3*D*, solid line), but the AN population does not show $EI_{max} > 0.9$ and does not show the increase in firing rate with CF (Fig. 3*E*), seen in the TB. Note that Fig. 3, *B*–*E*, clearly illustrates that the chinchilla, quite in contrast to the gerbil (21, Fig. 3), yielded a sizable number of TB and AN fibers with CF < 500 Hz.

Synchronization and Entrainment to Low-Frequency Tones off-CF

Some types of cochlear nucleus (CN) neurons in cat have excellent phase-locking in their tuning curve "tail" (43, 44, 52, 54), and R values in such tails are often higher than for neurons tuned to those low frequencies. A similar trend is also observed in the TB of gerbil (20). We examined whether chinchilla TB fibers also exhibit this trend. We systematically stimulated TB fibers in their low-frequency tail over a range of SPLs and frequencies. In fibers with low CF, frequencies higher than CF were occasionally tested.

The R_{max} values of bushy-type fibers stimulated at low frequencies are plotted in Fig. 4*A* (filled symbols) against their corresponding CF. R_{max} values at CF of these fibers are plotted in the background for comparison (Fig. 4*A*, empty circles, same data as in Fig. 3*A*). A total of 155 rate-level curves of bushy-type neurons were collected from 77 fibers: about half of these curves (76/155) were from 42

Downloaded from journals.physiology.org/journal/jn (081.164.135.205) on July 13, 2026.

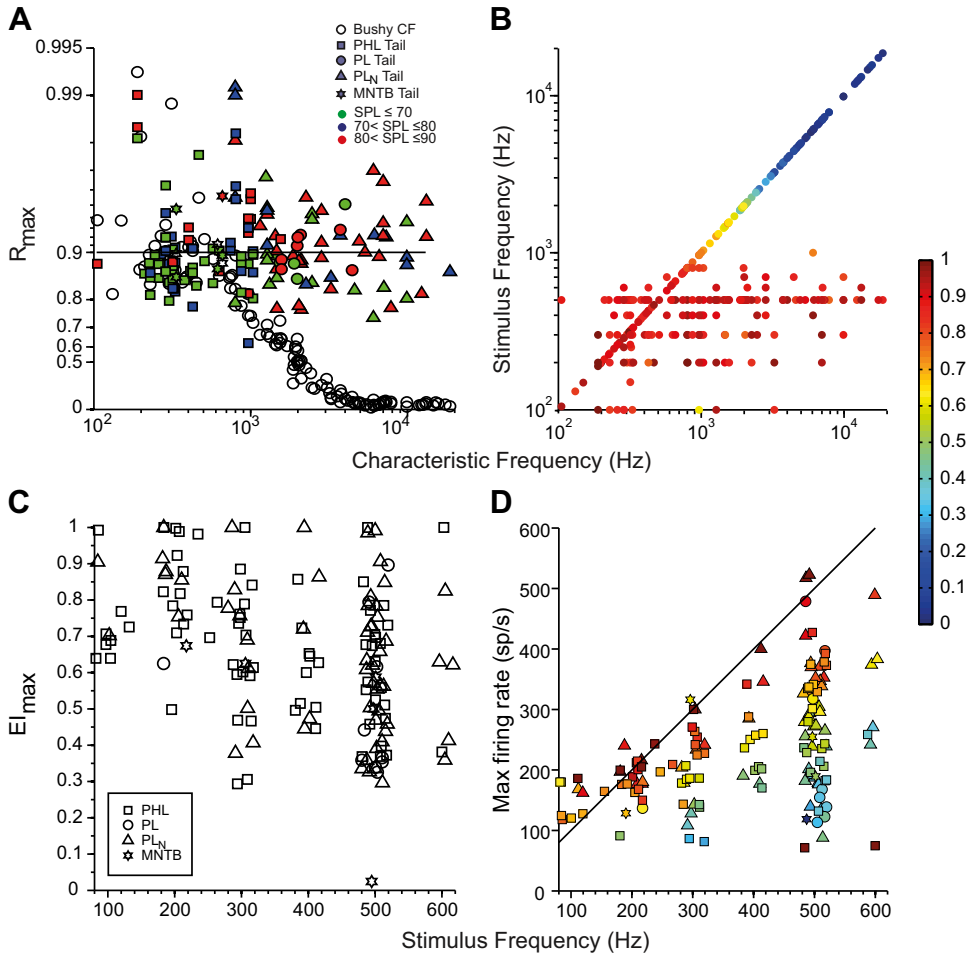


Figure 4. Strength of phase-locking and entrainment to off-CF tones for different types of TB fibers. *A*: R_{max} values of all bushy-type neurons in the chinchilla TB and MNTB, for stimuli at CF or off-CF (empty and solid, respectively), plotted against CF. Different colors indicate the SPL at which R_{max} is obtained (color code: see *inset*). The solid horizontal line indicates the "high-sync" criterion (R_{max} = 0.9). Neurons were sometimes tested at multiple frequencies, so that there can be multiple R_{max} values per neuron. For neurons that did not generate significant phase-locking to stimuli in the tuning curve tail, no R_{max} tail data point is shown. *B*: same data, with R_{max} color coded, to illustrate the stimulus frequencies used as a function of CF. *C* and *D*: entrainment of TB neurons to off-CF low-frequency stimuli. Abscissa values were slightly jittered to improve visualization. *C*: EI_{max} as a function of stimulus frequency for PHL, PL, PL_N, and MNTB recordings. *D*: maximum firing rate as a function of stimulus frequency, with EI_{max} color coded. A single fiber can contribute multiple data points. The number of fibers of each PSTH category was as follows: 32 PL_N, 10 PL, 34 PHL, and 3 MNTB. CF, characteristic frequency; EI_{max}, maximum value of entrainment index; MNTB, medial nucleus of the TB; PHL, phase-locked; PL, primary like; PL_N, primary-like-with-notch; TB, trapezoid body.

fibers with PL- and PL_N-type responses and the rest (79/155 curves) were from 23 fibers with PHL responses. Also, five rate-level curves were collected from three MNTB cells. Overall, a majority of the neurons stimulated at low frequencies had R_{max} value $\geq$ 0.9: such values were found in 7/13 rate-level curves from 6/10 PL fibers (Fig. 4*A*, filled circles); 32/63 rate-level curves from 20/33 PL_N fibers (Fig. 4*A*, triangles); 32/79 rate-level curves from 18/34 PHL fibers of which six fibers also had high-sync values at CF (Fig. 3*A*, squares); and 2/5 rate-level curves from 2/3 MNTB neurons (Fig. 4*A* stars).

The SPL range at which the R_{max} values were obtained was split into three groups indicated by colors of the filled symbols: green indicates SPL $\leq$70 dB, blue indicates 70 dB $<$ SPL $\leq$ 80 dB, and red indicates 80 dB $<$ SPL $\leq$ 90 dB. An elevated stimulus level is required to excite neurons at frequencies off-CF, particularly for high-CF neurons. However, Fig. 4*A* shows that even midrange levels ($\leq$ 70 dB, green) could yield R_{max} values $\geq$ 0.9. Figure 4*B* shows the stimulus frequencies used (ordinate) at the different CFs (abscissa), with color coding of R_{max} values (warm color = high R_{max}; cool color = low R_{max}, see color bar next to panels *B* and *D*). The diagonal of equality shows the data already shown in Fig. 3*A* for stimulus frequency equal to CF and the progression of hot to cool colors from low to high CFs reflects the low-pass shape in that figure. For the data points below the diagonal (stimulus frequency $<$ CF) as well as for the data points above it (stimulus frequency $>$ CF), it is clear that high R_{max} values are obtained across the whole range of CFs.

Again, we examined whether enhanced phase-locking is accompanied by high entrainment. Figure 4*C* shows EI_{max} as a function of stimulus frequency. Note that neurons were often tested at multiple off-CF frequencies so that a neuron can contribute multiple data points. Stimulation in the tail indeed produced responses with EI_{max} value $>$ 0.9 (9 fibers, 5 PL_N and 4 PHL), and this is also reflected in the pattern of firing rates close to the diagonal of equality (Fig. 4*D*). However, again the entrainment was not as prominent as observed in the cat (43, 44), and perfect entrainment (line of equality) was rather rare.

To better interpret the finding of enhanced phase-locking and high entrainment to low-frequency, off-CF stimuli in TB fibers (Fig. 4), we performed the same analysis on responses of AN fibers (Fig. 5, *A* and *B*). Indeed, a previous study in cat (44) shows that the criteria that indicate enhanced phase-locking and entrainment to STCF in TB fibers relative to AN fibers cannot simply be applied to responses to off-CF stimuli: in response to off-CF tones, even AN fibers could generate R_{max} and EI_{max} values $\geq$ 0.9. This is also the case in the chinchilla AN, where R_{max} values tended to be higher in response to low-frequency stimuli presented below CF (Fig. 5*A*, filled symbols) than in fibers tuned to these low frequencies (Fig. 5*A*, empty

Downloaded from journals.physiology.org/journal/jn (081.164.135.205) on July 13, 2026.

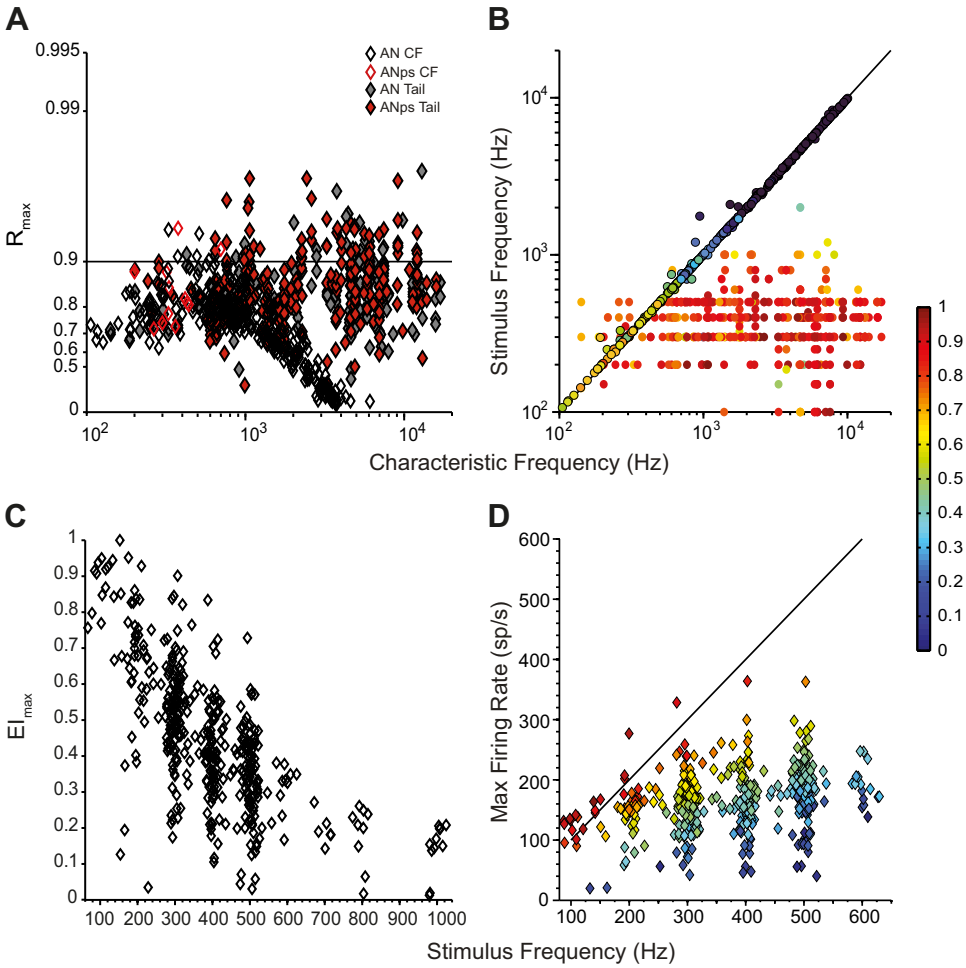


Figure 5. Strength of phase-locking and entrainment to off-CF tones in AN fibers. *A*: R_{max} values of AN fibers for stimuli at CF or off-CF (empty and solid, respectively), plotted against CF. Red symbols represent responses displaying peak-splitting. The solid horizontal line indicates the "high-sync" criterion (R_{max} = 0.9). Fibers were sometimes tested at multiple frequencies, so that there can be multiple R_{max} values per neuron. Fibers that did not generate significant phase-locking (either at CF or off-CF) are not represented. *B*: same data, with R_{max} color coded, to illustrate the stimulus frequencies used as a function of CF. *C* and *D*: entrainment of AN fibers to off-CF low-frequency stimuli. Abscissa values were slightly jittered to improve visualization. *C*: EI_{max} as a function of stimulus frequency. *D*: maximum firing rate as a function of stimulus frequency, with EI_{max} color coded. A single fiber can contribute multiple data points. AN, auditory nerve; ANps, AN fibers displaying peak-splitting; CF, characteristic frequency; EI_{max}, maximum value of entrainment index.

symbols), so values > 0.9 were not uncommon for CFs above 500 Hz (see also lack of "hot colors" along diagonal in Fig. 5*B*). Nevertheless, a comparison with Fig. 4*A* makes it clear that the pattern of R_{max} values in the AN is not simply reflected in TB and MNTB responses but that the latter values are increased relative to the AN. The same applies to measures of entrainment. EI_{max} values of AN fibers to off-CF low-frequency stimulation show a pattern that is quite different from TB

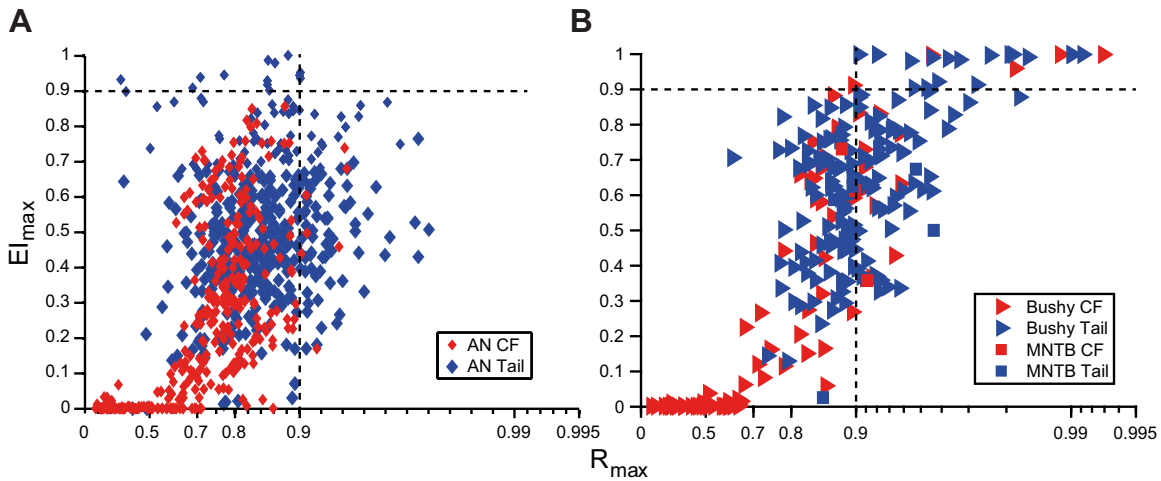


Figure 6. Relationship between EI_{max} and R_{max}. *A*: no obvious relationship between EI_{max} and R_{max} is observed in chinchilla AN. Data for response to CF tones are in red and to off-CF tones in blue. *B*: EI_{max} vs. R_{max} for chinchilla trapezoid body (TB) shows an association between high R_{max} and high EI_{max} values. Data for bushy-type neurons to CF-tones are shown with red triangles and to off-CF stimuli with blue triangles. Similarly, square symbols indicate data for MNTB responses. Only data with significant R values are shown. The dashed vertical and horizontal lines indicate R_{max} and EI_{max} values of 0.9. AN, auditory nerve; CF, characteristic frequency; EI_{max}, maximum value of entrainment index; MNTB, medial nucleus of the TB.

Downloaded from journals.physiology.org/journal/jn (081.164.135.205) on July 13, 2026.

fibers (Fig. 5*C* vs. Fig. 4*C*), and the same holds for maximal firing rate (Fig. 5*D* vs. Fig. 4*D*). Thus, TB fibers respond to off-CF, low-frequency tones with larger values of phase-locking and entrainment, than AN fibers.

Figure 6 summarizes the AN (Fig. 6*A*) and TB (Fig. 6*B*) data. The horizontal and vertical dashed lines indicate the 0.9 values that have previously been used as simple upper bounds delimiting R_{max} and EI_{max} values to STCF in the AN (20, 43). In the TB, there is an association between R_{max} and EI_{max} values so high entrainment is found in fibers with high phase-locking (Fig. 6*B*). In the AN, this quadrant (with R_{max} and $EI_{max} > 0.9$) is empty. Note that the clustering of values on the abscissa ($EI_{max} = 0$) is expected and reflects the poor synchronization at CFs above a few kilohertz, where entrainment is impossible because of refractoriness.

Peak Splitting

In many instances, we observed complex phase-locking behavior. This is illustrated with cycle dot rasters in Fig. 7 for responses of three neurons with different CF to a 300-Hz tone over a range of SPLs, and in the bottom row with a combination of measures of average rate (left ordinate, spikes/s) and phase-locking (R and phase, right ordinate). In cycle dot rasters, each spike is represented as a dot positioned as a function of its phase in the stimulus cycle, where the different horizontal stacks at a given SPL represent successive stimulus cycles (bottom: first cycle, top: last cycle). In Fig. 7, the abscissa spans two cycles to facilitate viewing. The fiber with the lowest CF (Fig. 7, left column) shows phase changes at high SPL: the response changes from a single mode at 75 dB to one with multiple modes at 80 and 85 dB, to then return to a single mode at 90 dB at an earlier phase than at 75 dB. These changes are reminiscent of descriptions in the chinchilla AN (64). However, complex modes of phase-locking are also observed in this fiber at low SPL, near the rate threshold. Even more complex changes, sometimes including triple modes, are visible in the responses of the two other fibers illustrated (Fig. 7, middle and right columns). Note that the phase behavior is rather stable as a function of post-stimulus time: the distribution of dots within each raster is the same for the bottom and top rows, so it is not the case that peak-splitting builds up or changes over time with subsequent cycles of the tonal stimulus. These complex phase-locking patterns are reflected in erratic R and phase values (Fig. 7, bottom row) and can include high R_{max} values (R_{max} = 0.86, 0.9, 0.92, respectively, indicated by arrowheads).

Peak-splitting was rare to CF tones but was rampant to off-CF stimulation. The R_{max} data of Figs. 3*A* and 4*A* are replotted in Fig. 8*A* (response to CF tones) and Fig. 8*B* (response to off-CF tones) with an indication (red symbols) of whether peak-splitting was observed at any of the SPLs tested. There are only 4/83 fibers with peak-splitting to CF tones (Fig. 8*A*), whereas about half of the fibers studied (36/76) showed peak-splitting when stimulated in their tuning curve tail (Fig. 8*B*), frequently at moderate SPLs (~45–70 dB). Peak-splitting is not a necessary condition to obtain high R_{max} values, as such values are also observed in fibers that do not display peak-splitting (Fig. 8, black symbols). We could not discern a clear pattern regarding the presence of peak-splitting with response type, CF, or R_{max} value.

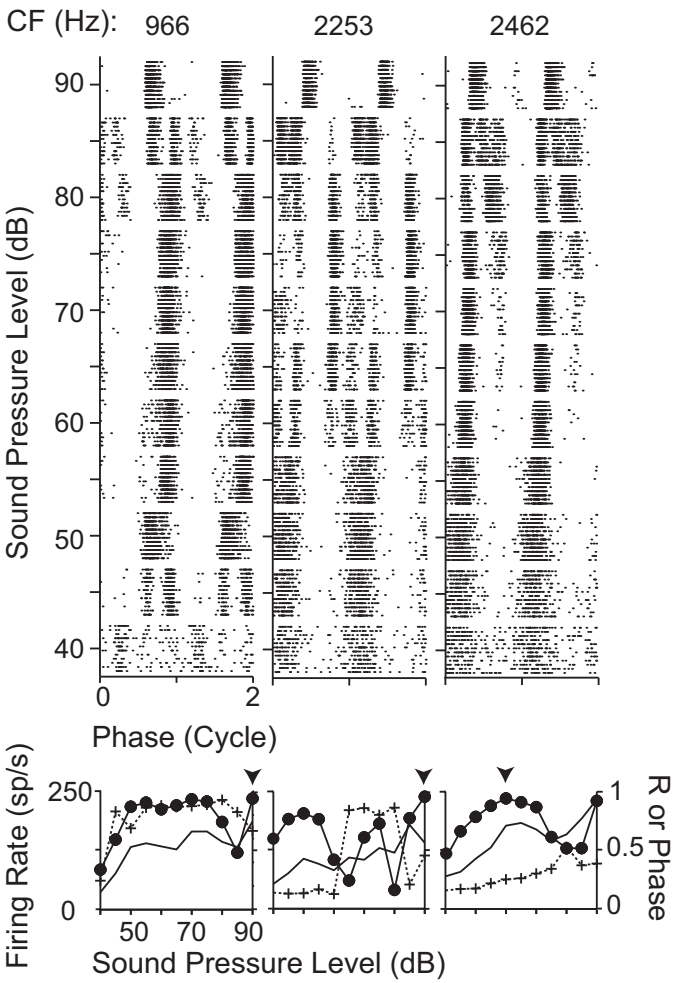


Figure 7. Various manifestations of peak-splitting in three chinchilla TB fibers. Each column shows the responses of one fiber, arranged for increasing CF (stated above each column) from left to right. The stimulus was a 300-Hz tone, varied over the range of SPLs indicated by the ordinate. The dot rasters show the occurrence of spikes as a function of stimulus phase. For ease of viewing, two cycles are shown, i.e., the responses are "folded" at twice the stimulus period. The analysis window excludes the first 10 ms of the response. At each SPL, the different rows of dots correspond to subsequent cycles of the stimulus. The stimuli were repeated 100 times: data for different stimulus repetitions are plotted on top of each other. The fiber with CF near 1 kHz had a PHL response pattern at CF; the two other fibers had PL_N responses. Below each column of dot rasters, average rate (solid line, left ordinate), and phase-locking magnitude (R, circles, right ordinate) and phase (+ symbols, right ordinate) are shown. R_{max} for each neuron is indicated by an arrowhead (R_{max} = 0.86, 0.9, and 0.92, respectively). The scale and range of the axes are identical for all panels. CF, characteristic frequency; PHL, phase-locked; PL_N, primary-like-with-notch; SPL, sound pressure level; TB, trapezoid body.

To evaluate whether peak-splitting reflected pre- or post-synaptic mechanisms, we also studied peak-splitting in AN responses. Peak-splitting to CF-tones was observed in only 12/329 fibers (Fig. 5*A*, red open symbols). In the low-frequency tail, peak-splitting was more prevalent, with 257/457 datasets (obtained from 58/154 fibers) showing peak-splitting (Fig. 5*A*, red solid symbols). Although peak-splitting to CF tones only occurred at high SPLs (≥85 dB, with one exception at 75 dB), in the tail of tuning curves, it could occur at much lower SPLs, as was also seen in TB fibers (Fig. 7).

Downloaded from journals.physiology.org/journal/jn (081.164.135.205) on July 13, 2026.

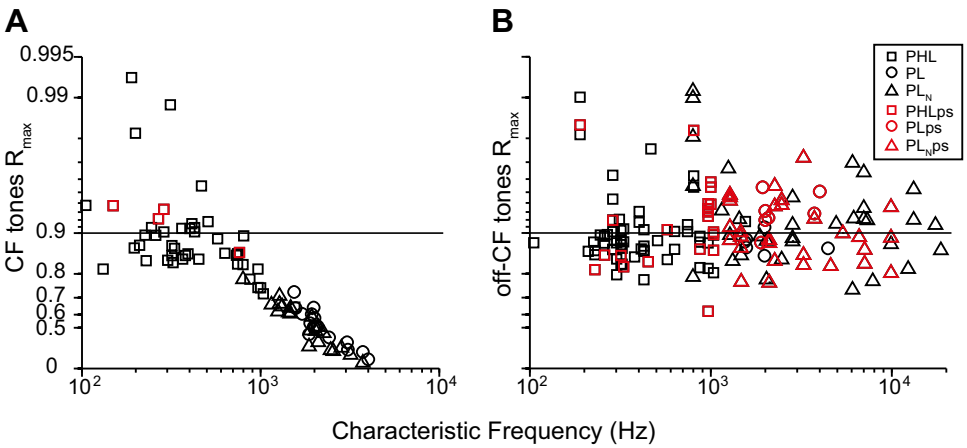


Figure 8. R_{max} values of TB fibers to CF-tones (*A*) and off-CF tones (*B*), with indication of presence or absence of peak-splitting (red and black symbols, respectively). Peak-splitting occurred in 4/83 fibers to CF-tones (*A*), and in 36/76 fibers to off-CF tones (*B*). The horizontal line at R_{max} = 0.9 marks the "high-sync" criterion. Each symbol in *A* corresponds to one fiber; in *B*, one fiber can contribute several datapoints. CF, characteristic frequency; PHL, phase-locked fibers; PHLps, PHL fibers displaying peak-splitting; PL, primary-like fibers; PLps, PL fibers displaying peak-splitting; PL_N, primary-like-with-notch fibers; PL_N fibers displaying peak-splitting; TB, trapezoid body.

Other Basic Properties of TB Fibers

Although not the primary purpose of our data collection, a number of general properties of chinchilla TB fibers are worth reporting. The majority of fibers found in the chinchilla TB had low thresholds, plotted in Fig. 9*A*, as estimated at CF from the threshold tuning curve. The dashed line indicates the chinchilla audiogram (65), and the solid black line indicates the average threshold for AN fibers (36). The majority of TB fibers (106/138) had a minimum threshold below 20-dB SPL. A contributing factor to the low thresholds at low CFs may be the opening of the bullas (66). There is no obvious separation of thresholds between different response types.

The distribution of SR (Fig. 9*B*) shows a very wide range from 0 to almost 180 spikes/s seemingly independent of CF. Fibers with CHOP (average = 9 spike/s, $n = 5$, diamonds) and O responses (0.4 spikes/s, $n = 5$, + symbols) are clearly associated with low SR values. There was no correlation between SR and threshold at CF (not shown).

Figure 9*C* shows Q_{10} values derived from threshold tuning curves as in Fig. 1*A*. The symbols indicate the Q_{10} values for different response types and the red dotted line in the graph shows the average Q_{10} value of chinchilla AN fibers (66, Fig. 4). As in the AN, the Q_{10} values of TB fibers increase with CF.

The minimum peak latency of responses to CF tones shows an orderly decrease from low to high CF (Fig. 9*D*). There is no clear segregation between neurons with PL and PL_N responses at the CFs (> 1 kHz) where these PSTH patterns can be distinguished. The latency values and pattern

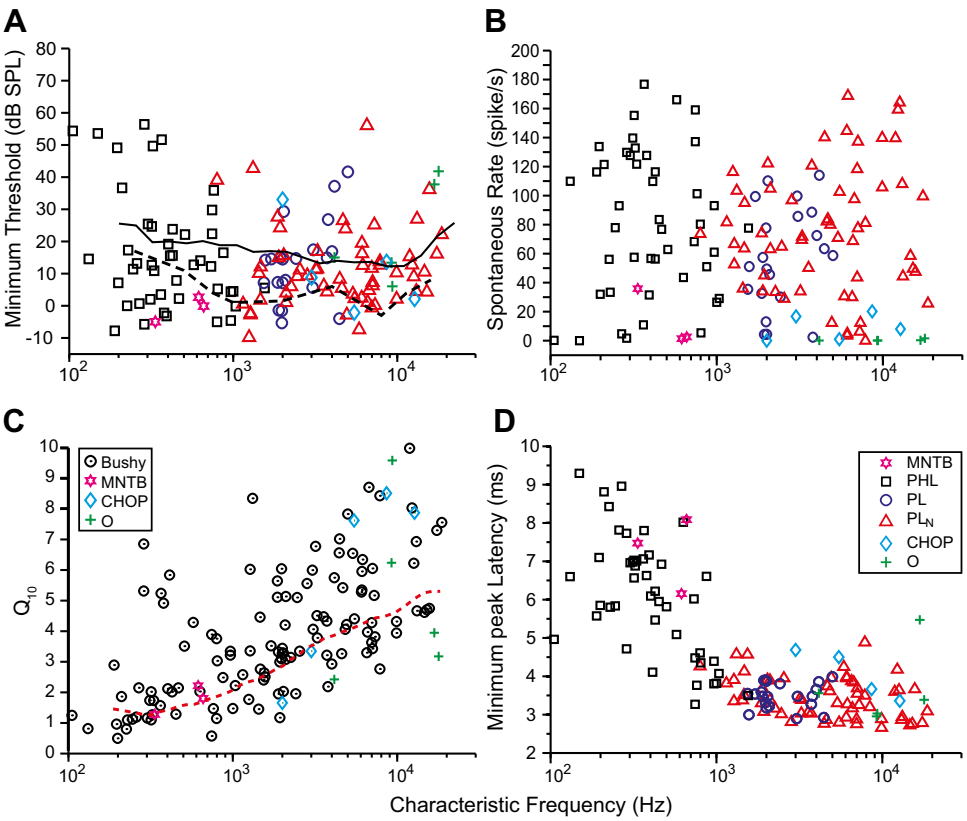


Figure 9. Some basic properties of TB fibers recorded in the chinchilla. *A*: graph shows minimum threshold from frequency-threshold tuning curve (i.e., threshold at CF) versus CF. The black solid line is the average threshold for AN fibers with high spontaneous rate (36). The dashed black line is the behavioral threshold (65). *B*: distribution of spontaneous firing rate as a function of fiber CF. *C*: sharpness of tuning versus CF. The red dotted line indicates average value of Q_{10dB} of AN fibers with high spontaneous rate (36). *D*: minimum peak latency against CF for different unit response types, indicated by different symbols (see *inset*). AN, auditory nerve; CF, characteristic frequency; CHOP, chopper; O, onset; PHL, phase-locked; PL, primary-like; PL_N, primary-like-with-notch; TB, trapezoid body.

Downloaded from journals.physiology.org/journal/jn (081.164.135.205) on July 13, 2026.

with CF are consistent with expectations for this level of the auditory system but do not provide further clues to disambiguate the parent cell type of the recordings, in casu do not help to differentiate cell types at low CFs.

Nonmonotonic Rate-Level Functions

In examining the responses to CF tones, we noticed that in some cases, the firing rate decreased with increasing SPL. We separated rate-level functions into monotonic and nonmonotonic cases (see METHODOLOGY) for the different response types (Fig. 10). Of the total population, PHL fibers had the largest fraction (51%) of nonmonotonic rate responses, followed by PL_N fibers (36%). For monotonic responses (Fig. 10, left column), maximal firing rates were lower for PL fibers than for PL_N fibers ($P < 0.001$), and the same holds for PHL compared with PL_N ($P < 0.001$, Matlab two-sample t test). As was illustrated above (Fig. 7), peak-splitting behavior can be accompanied by changes in firing rate. However, peak-splitting was not commonly observed in response to tones at CF (Fig. 8*A*). The large number of nonmonotonic rate-level functions in the group with PHL responses must therefore reflect another mechanism, most likely inhibition (67–69).

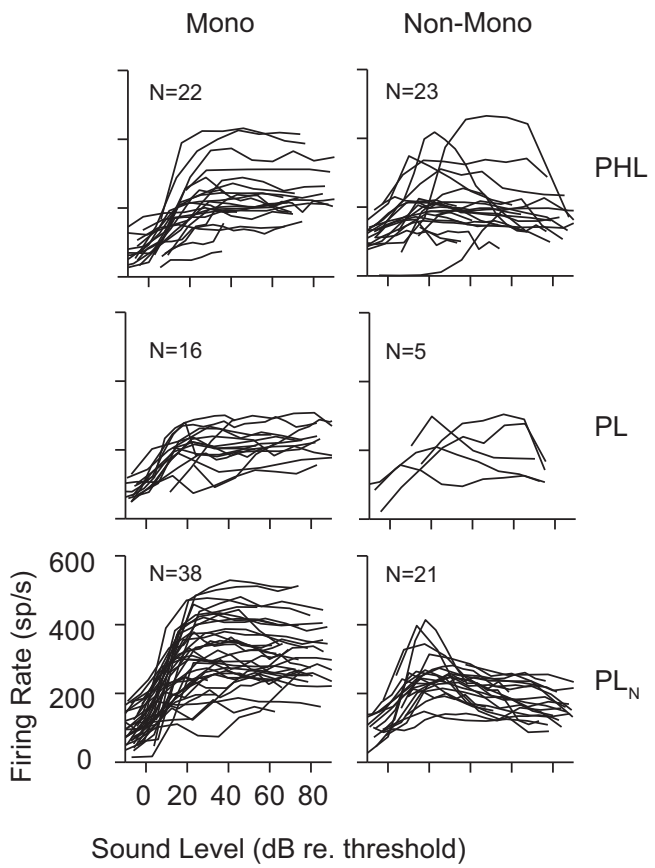


Figure 10. Rate-level curves at CF for three different response types, sorted into monotonic (left column) and nonmonotonic (right column). Scales for ordinate and abscissa are the same for all panels and are indicated in the *bottom left*. Abscissa is normalized to threshold at CF, obtained from the threshold tuning curve of each neuron. CF, characteristic frequency; PHL, phase-locked; PL, primary-like; PL_N, primary-like-with-notch.

Interaural Attenuation

One concern when using small mammals for binaural studies is acoustic cross talk between the two ears. This concern is exacerbated by the surgical opening of the bulla(s) needed to gain access to the ventral brainstem. We used rate-level curves at CF to measure interaural attenuation by applying the same stimulus sequentially to the two ears and quantifying the shift between the resulting rate-level curves. Because these monaural neurons could be driven by either the contra- or ipsilateral ear, we refer to the "driving" ear as the ear giving the lowest threshold and the "non-driving" ear as the ear giving the highest threshold. For each of the monaural neurons, we measure the shift in SPL between corresponding points in the rate-level curves. Examples are shown in Fig. 11, *A–D*, where the solid line is the rate-level curve obtained from stimulation of the driving ear and the dashed line is that of the nondriving ear. Circles in the graphs indicate the points in the rate-level curve at which the attenuation is measured, and the dotted horizontal line shows the interaural attenuation measured in decibels. Due to the upper limit of stimulation of 90 dB SPL, a corresponding point could not always be identified for the nondriving ear (e.g., Fig. 11*A*); in these cases, only a lower limit could be derived. For the four examples illustrated, the interaural attenuation varied from 43 (the lowest value in our sample) to 78 dB.

Figure 11*E* shows the interaural attenuation measured for 45 monaural TB fibers (filled circles) and 12 lower bounds (empty triangles). The vast majority of values were >50 dB, but a cluster of neurons with CF near 3–4 kHz showed values between 40 and 50 dB. There is an inverse trend with larger attenuation at low than at high frequencies ($r = -0.40$, $P < 0.009$).

DISCUSSION

We developed a ventral transbulla approach to collect population data of monaural axons bundled in the TB of the chinchilla. The rationale for taking this approach is that TB recordings provide an excellent window into the properties of the axons feeding into the binaural nuclei of the SOC. Extracellular recordings in the CN, particularly when studying responses to low frequencies in its rostral pole, are hampered by large field potentials, which make the physiological isolation of single units difficult. The TB lacks a tonotopic layout and the associated field potentials. Moreover, axonal recordings with high-impedance, sharp micropipettes result in clean all-or-none spikes and are little affected by field potentials. Finally, previous studies have shown that these types of TB recordings sample predominantly though not exclusively axons of bushy cells (56, 57, 61, 70, 71). These advantages are particularly relevant when studying the property of interest here: phase-locking to fine-structure.

Enhanced Phase-Locking at Low CF

We collected TB responses to pure tones over a wide range of SPLs, not only at CF but also at non-CF frequencies, mostly in the tuning curve "tail." Moreover, we obtained AN responses to the same stimuli. Use of the same experimental approach as previously used in cat and gerbil is advantageous to compare basic features of phase-locking to fine-structure not only

Downloaded from journals.physiology.org/journal/jn (081.164.135.205) on July 13, 2026.

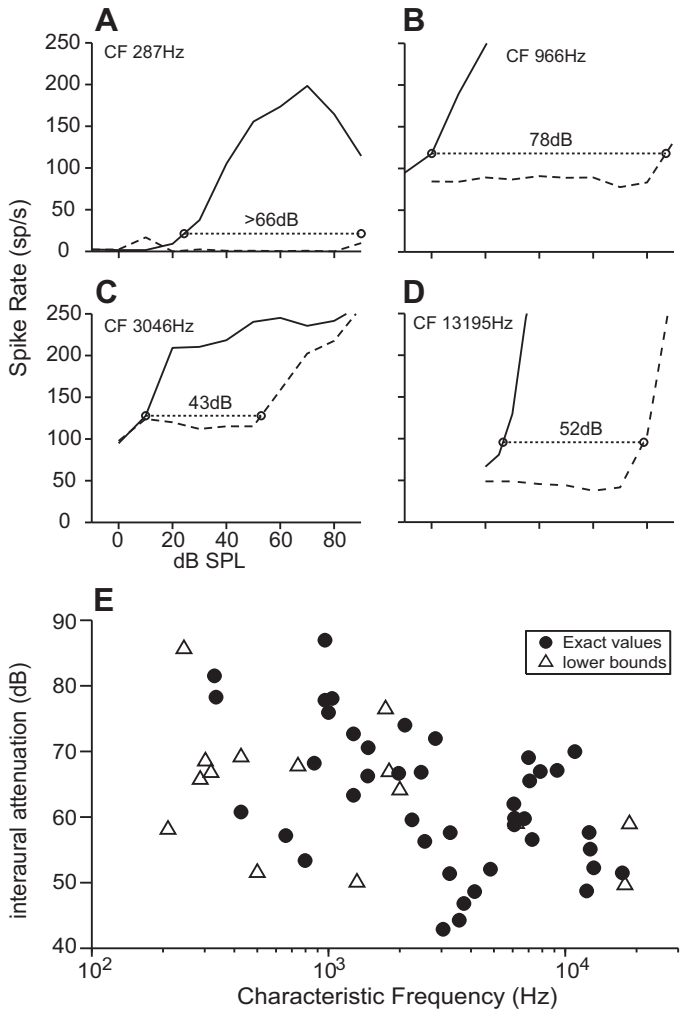


Figure 11. *A–D*: examples of interaural attenuation values (dotted line) measured in four neurons with rate-level curve recorded at CF from the driving ear (solid line) and nondriving ear (dashed line). The horizontal lines with circles indicate the quantification of interaural attenuation. *E*: interaural attenuation values for 41 monaural fibers (Bushy type $n = 37$; CHOP $n = 1$; MNTB $n = 2$; O $n = 1$) plotted against their CF. Lower bound values of 12 monaural fibers are plotted with triangle symbols (Bushy type $n = 10$; CHOP $n = 1$; O $n = 1$). CF, characteristic frequency; CHOP, chopper; MNTB, medial nucleus of the trapezoid body.

across AN and TB but also across species. We found that chinchilla TB fibers display enhanced phase-locking to low-frequency tones relative to AN fibers. Qualitatively, this enhancement showed features similar to observations in the cat, such as temporal adaptation (Fig. 1, *B–D*), enhancement both at CF and in the tuning curve tail, and both in terms of increased vector strength and entrainment (Figs. 3, 4, and 6). But there are quantitative differences with the cat in several respects.

Phase-locking to tones at CF in TB and AN from the three species is summarized in Fig. 12. Regarding TB fibers (Fig. 12*A*), the cat (red dots) shows the most consistent trend toward enhanced phase-locking for CF tones. The chinchilla recordings yield a bigger sample of fibers with very low CF. A few of these fibers show very strong enhancement in line with the cat data, but most fibers have only moderately enhanced phase-locking: their R_{max} values exceed the trendline for AN fibers (green dotted line) but straddle the high-sync criterion at $R = 0.9$. In cat, ~ 75% of fibers with CF < 700 Hz had enhanced phase-locking to CF tones, whereas in the chinchilla, it was somewhat less than 50%. The gerbil

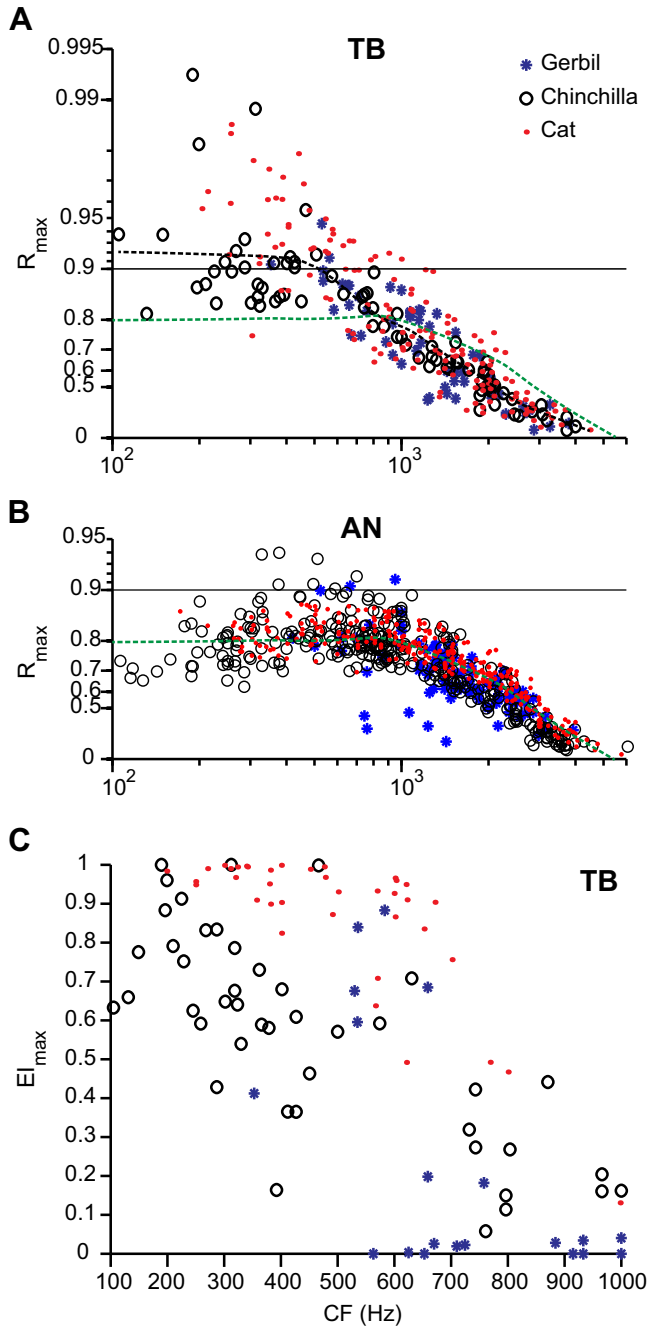


Figure 12. Direct synchronization (R_{max}) comparison of TB and AN between gerbil, chinchilla, and cat. *A*: significant R_{max} values of bushy-type TB fibers in gerbil (20, blue asterisks), chinchilla (empty circles), and cat (43, red dots). Dashed black line is TB trendline from combined data on the plot (lowess, span 30%), dashed green line is AN trendline from combined data in *B* (lowess, span 30%). *B*: R_{max} values at or near CF from responses obtained in AN of gerbil (17, blue asterisks), chinchilla (38, empty circles), and cat (3, red dots). The dashed green line is the same as *A*. The horizontal line at $R_{max} = 0.9$ marks the "high-sync" criterion in both graphs. *C*: EI_{max} values of bushy-type fibers at CF in the TB from three species (same symbols as for *A*). AN, auditory nerve; CF, characteristic frequency; EI_{max}, maximum value of entrainment index; TB, trapezoid body.

Downloaded from journals.physiology.org/journal/jn (081.164.135.205) on July 13, 2026.

data are largely in line with the cat and chinchilla data but the lack of fibers with CF < 500 Hz limits the presence of enhanced phase-locking to CF tones.

At the level of the AN, differences between the three species are less marked (Fig. 12*B*). Chinchilla AN fibers extend to lower CFs than in cat, and in turn, the cat data extend to lower CFs than in gerbil, but where CFs overlap, the distributions of R_{max} values are reasonably coextensive among the three species. The gerbil shows some outliers with poor phase-locking near 1 kHz. Between 300 Hz and 1 kHz, there are some AN fibers in gerbil and chinchilla with $R_{max} > 0.9$. The trendline fit to the aggregate data (green dotted line) shows a low-pass shape with corner frequency near 1 kHz.

Frequency Range of Phase-Locking

Phase-locking to the fine structure of sounds has been proposed as an essential neural property for a range of auditory percepts in humans (72), but this is not generally accepted (73). One point of contention is the frequency range of phase-locking in humans, which is thought by some to extend up to frequencies as high as 8–10 kHz (72, 74, 75) but is thought by others to be much more limited (76). We have argued that the study of bushy cells and their target cells has a prominent role in this debate (77). The first reason is that of all CN populations studied, bushy cells show the highest upper-frequency limit of phase-locking (for references, see Ref. 77). The second reason is that bushy cells feed into the binaural system and that the only auditory percepts for which the use of phase-locking to fine-structure is undisputable are binaural. For example, pure tones of slightly different frequencies to the two ears generate various manifestations of "binaural beating," both psychophysically (78, 79) and physiologically (80). In humans, the exquisite behavioral sensitivity to temporal differences between the ears ends abruptly at ~1.3 kHz, and the mechanisms underlying this "brick wall" limit are poorly understood (23). Chinchillas provide a unique opportunity to study such questions, not only because of their excellent low-frequency hearing but also for several technical reasons. Systematic study of both output and input of the binaural nuclei in the SOC is possible because of their enormous middle ear cavities, which enable routine axonal recording from outputs of the superior olivary complex via the lateral lemniscus (41) and their inputs via the trapezoid body (this study). Moreover, chinchillas have been extensively used in behavioral studies (81), even including in-ear stimulation (82), holding the promise of dichotic studies that could tighten the relationship between physiology and behavior.

We found that phase-locking in bushy cells of the chinchilla extends to 4 kHz (Fig. 3*A*). The general relationship to phase-locking in the AN, measured with pure tones at CF, is very similar to that observed in cat (43) and gerbil (20): enhanced at low frequencies but poorer at mid frequencies, with a crossover point somewhat below 1 kHz (red and dotted lines in Fig. 3*A*). The reduction at mid frequencies relative to the AN is of interest for the debate on the perceptual role and extent of phase-locking to fine-structure. It is sometimes suggested that weak AN phase-locking near or above the 4 kHz "limit" may be strengthened in the CNS because of the convergence of AN fibers on single CN neurons. Although such strengthening obviously occurs at low frequencies, we are not aware of any evidence of strengthening at mid-frequencies, where the AN fibers gradually lose coding of temporal fine structure with increasing CF. The reasons for this weakening of phase-locking in bushy cells, relative to AN fibers, are not known but likely involve temporal smearing from converging inputs and/or temporal limitations imposed by membrane properties. In any case, the upper limits of phase-locking in CN neurons are lower than those in the AN, not higher. As already mentioned, of all cell groups that have been examined in the cochlear nucleus, bushy cells show the strongest phase-locking over the widest CF range, when measured with vector strength of responses to CF tones. Thus, if the phase-locking range of bushy cells is not extended relative to the AN, it is not likely to be extended in any other neuronal population.

Entrainment

We observed that TB fibers not only show enhanced phase-locking but also entrainment (Fig. 3, *B* and *C*). However, high entrainment to tones at CF was much less common in chinchilla than in cat TB fibers (Fig. 12*C*). In the AN, high entrainment does not occur in response to CF tones (Fig. 3, *D* and *E*). It is intuitive that an increase in vector strength, which indicates a reduction in temporal jitter of spike times relative to the sound waveform, benefits temporal comparisons performed by binaural neurons in the brainstem. Perhaps less intuitive is that entrainment is also an important component of "enhancement" of phase-locking between AN and TB. Basically, each spike in the monaural afferents to the binaural nuclei is a marker of the acoustic waveform at each ear. Entrainment increases the reliability of a spike train as a series of such markers because it decreases the "cycle-skipping" that is observed in AN responses to low-frequency stimuli (2, 83). Thus, the number of coincidences between spike trains of two CF-matched cells with high entrainment (e.g., one bushy-type response from each ear) is higher than for two CF-matched AN fibers (84). A case in point is ITD sensitivity in the barn owl, which extends to much higher frequencies than in mammals. Indeed, the upper limit of phase-locking in monaural afferents to nc. laminaris is near 10 kHz (85), more than an octave above the limit in mammals. At such frequencies, the refractory period [~0.7–1 ms in TB fibers (86)] is much longer than the stimulus period, so phase-locked spikes are necessarily separated by interspike intervals of multiple periods. A robust neural representation of the waveform at each ear thus necessitates a high number of convergent monaural afferents, which is indeed observed [~45–150 from each side, (87)]. In contrast, mammalian binaural nuclei appear to favor a smaller number of monaural afferents with individual afferents making multiple synaptic contacts along extensive dendrites (84, 88–90). Entrainment fits into this scheme as a mechanism for reducing the need for convergence (84). There are additional factors to consider besides entrainment and number of afferents, such as the probabilistic nature of synaptic release and the presence of multiple synapses per fiber (90–93).

Enhanced Phase-Locking and Entrainment to off-CF Tones

Off-CF stimulation with a low-frequency tone resulted in high R_{max} values in high-CF TB fibers (Fig. 4*A*), and such off-CF tones generated entrained responses more frequently than

Downloaded from journals.physiology.org/journal/jn (081.164.135.205) on July 13, 2026.

CF tones (Fig. 4, *C* and *D*). The high R_{max} values observed in TB fibers to off-CF tones may partly originate peripherally: indeed, the upper boundary of R_{max} values to such tones increases with CF in the AN (Fig. 5*A*). However, responses that are both highly entrained and phase-locked (R_{max} and $EI_{max} > 9$) were only observed in the TB, particularly in response to stimulation in the tail (Fig. 6*B*, blue symbols), so that these properties cannot be entirely inherited from the AN.

A common observation is that high-CF binaural neurons can show ITD sensitivity when stimulated with tones in their low-frequency tail (11, 27, 94), and enhanced phase-locking such as observed here may contribute to that sensitivity. However, in response to wideband stimuli such as noise, with multiple frequency components interacting in the spectral filters of the monaural afferents, the components near CF dominate (27, 28, 95), and the functional role of enhanced phase-locking in the low-frequency tail is less clear for such stimuli.

There is only one previous study in chinchilla that we are aware of that compared phase-locking and entrainment to fine-structure between VCN cells and AN. That study (38) examined these two properties for responses to both CF and off-CF tones for a more restricted range of CFs (<1,500 Hz) and levels (mostly 60 dB SPL). Its findings are consistent with ours and also led to the conclusion that "high-sync" responses and high entrainment are observed in the CN of the chinchilla but are somewhat more limited than in the cat, both in terms of their CF distribution, their frequency distribution, and the degree of enhancement of these features relative to the AN.

Peak-Splitting

A surprising finding was the common occurrence of "peak-splitting" in TB fibers, particularly in response to off-CF tones (Fig. 8). Peak-splitting was first observed in AN fibers in cat (96): it is an elusive phenomenon of unclear origin (97, 98), which consists of several features that tend to co-occur (multimodal period histograms, phase-shifts, and changes in average firing rate). In cat, it occurs at SPLs near 90 dB or higher both to tones at CF and to tones in the tail of the tuning curve, for CFs up to a few kilohertz (44, 99, 100). Similar complexities have been observed in cat TB fibers (43, 61), also at high SPL.

In chinchilla TB fibers, peak-splitting was common, particularly in response to off-CF tones (Fig. 8*B*), and was observed not only at high SPLs but also at much lower SPLs than in TB fibers in the cat, even extending to near-threshold levels (Fig. 7). Also, it was observed over a wider range of CFs than in cat, extending up to ~10 kHz. At the level of the TB, peak-splitting can reflect a multitude of mechanisms, including the convergence on the parent cell of inputs with unimodal phase-locking but with differences in latency, as can arise, e.g., from differences in CF or effective conduction time. Also, in vitro studies have shown the firing of multiple spikes of some bushy cells to a depolarizing input (101, 102). Our AN data however suggest that peak-splitting in the TB mainly reflects peak-splitting already present in inputs from the AN to neurons projecting into the TB. Indeed, compared with the cat (44), peak-splitting was common in chinchilla AN fibers stimulated in their tuning curve tail (Fig. 5*A*). This is consistent with other data obtained in chinchilla. Complex phase-locking behavior was reported in chinchilla AN over a very wide range of CFs (31, 64), although in these studies, the tones were of very low frequency ("bias" tones of a few 100 Hz or even lower). Also, axonal recordings from presumed MSO neurons show reduced ITD sensitivity to pure tones for frequencies <400 Hz (41), and unpublished data from our laboratory suggest that peak-splitting may be a contributing factor. These findings in chinchilla data are reminiscent of findings in gerbil (see discussion in Ref. 20), where peak-splitting is also prevalent at several anatomical levels and is able to impact ITD sensitivity in MSO neurons. The difference between these two rodent species and cat hints that the "clean" phase-locking and ITD sensitivity in cat, across a wide range of frequencies and intensities, is not a trivial outcome of cochlear transduction and anatomical wiring but involves specialized mechanisms that are perhaps less well developed in rodents.

Identity of Neurons Recorded

Our recordings targeted the TB, and on anatomical grounds, must be derived predominantly from the output fibers of the AVCN. This is supported by their PSTHs. Out of 135 fibers recorded, the largest group ($n = 59$, 44%) showed PL_N responses. This is as expected as the PL_N pattern is associated with globular bushy cells, which have larger caliber axons and are oversampled in axonal recordings (57, 61, 70). Only 15% ($n = 21$) of the fibers displayed the PL response pattern associated with spherical bushy cells. A third of the recordings ($n = 45$) were classified as having the PHL pattern. Although this was our main targeted population in view of our interest in characterizing temporal coding of fine structure in monaural afferents to the SOC, it is unfortunately a group for which the PSTH is not a good basis to infer morphological cell class. Virtually all neurons of the cochlear nucleus show some degree of phase-locking to pure tones, albeit with different upper cutoff frequencies at which this property is lost. Phase-locking masks the PSTH patterns that enable categorization of cells, and it prevents their assignment to presumed morphological cell classes. In view of previous labeling studies and the composition of the TB (57, 61, 70), there is little doubt that most cells in this group are bushy cells, but the relative proportion of globular versus spherical bushy cells is unknown. This limits a mechanistic understanding of binaural physiology because of the opposite sign of the two bushy cell classes: inhibitory (via the MNTB) for globular and excitatory for spherical bushy cells. The only handle giving some insight into cell composition is the small number of recordings ($n = 3$) from low-CF MNTB neurons. Because of their monosynaptic innervation by globular bushy cells through the powerful calyx of Held, the responses of MNTB neurons are virtually indistinguishable from those of globular bushy cells, but they can be identified extracellularly through the prepotential generated by the calyx (86, 103). It is interesting to observe that the small sample of MNTB neurons had low SR values (Fig. 9*B*, $n = 3$, 13 spikes/s). Combining the fibers with PL_N responses and MNTB neurons (stars and triangles), a possible though speculative interpretation of the data is that globular bushy cells show an increase in SR with CF, as observed with more direct evidence in the cat (56, 61). This

Downloaded from journals.physiology.org/journal/jn (081.164.135.205) on July 13, 2026.

would imply that low-CF high-SR fibers are dominantly of the spherical bushy type (57, 104).

A small number (each $n = 5$) of CHOP and O responses was observed as well. These are associated with nonbushy cell types. The CHOP responses are likely derived from AVCN type I multipolar cells: these cells are numerous but have thin axons, which is thought to account for their limited sampling (71). The finding of O responses in these TB recordings, although small in number, is intriguing. One of the O neurons had poor timing of the onset response, had high threshold and wide frequency tuning, and is of unsure origin. The other four O responses were of the O_L variety (52), i.e., with a well-timed onset and a low level of sustained activity. Such responses can be recorded from the octopus cell area (OCA) in the PVCN. Even though the output of the OCA is classically thought to emanate through the intermediate acoustic stria (IAS) (105), single neuron labeling has shown a number of neurons projecting via the TB (106, 107), and we have recent evidence that these OCA neurons constitute a class of projection cells that is separate from octopus neurons (108).

DATA AVAILABILITY

Data will be made available upon reasonable request.

ACKNOWLEDGMENTS

We thank Drs. Tom Franken and Abel Jonckheer for support with software and hardware.

GRANTS

This work was funded by Fonds Wetenschappelijk Onderzoek (Research Foundation Flanders) grants G.0A11.13 and G.091214N and Bijzonder Onderzoeksfonds KU Leuven (grant BOF OT-14–118) to P.X.J.

DISCLOSURES

No conflicts of interest, financial or otherwise, are declared by the authors.

AUTHOR CONTRIBUTIONS

L.W. and P.X.J. conceived and designed research; L.W., E.V., and P.X.J. performed experiments; L.W., E.V., and P.X.J. analyzed data; L.W., E.V., and P.X.J. interpreted results of experiments; L.W. and E.V. prepared figures; L.W. and P.X.J. drafted manuscript; L.W. and P.X.J. edited and revised manuscript; P.X.J. approved final version of manuscript.

REFERENCES

1. **Kiang NY**, **Pfeiffer RR**, **Warr WB**, **Backus AS.** Stimulus coding in the cochlear nucleus. *Trans Am Otol Soc* 53: 35–58, 1965.
2. **Rose JE**, **Brugge JF**, **Anderson DJ**, **Hind JE.** Phase-locked response to low-frequency tones in single auditory nerve fibers of the squirrel monkey. *J Neurophysiol* 30: 769–793, 1967. doi:10.1152/jn.1967.30.4.769.
3. **Johnson DH.** the relationship between spike rate and synchrony in responses of auditory-nerve fibers to single tones. *J Acoust Soc Am* 68: 1115–1122, 1980. doi:10.1121/1.384982.
4. **Joris PX**, **van der Heijden M.** Early binaural hearing: the comparison of temporal differences at the two ears. *Annu Rev Neurosci* 42: 433–457, 2019. doi:10.1146/annurev-neuro-080317-061925.
5. **Goldberg JM**, **Brown PB.** Response of binaural neurons of dog superior olivary complex to dichotic tonal stimuli: some physiological mechanism of sound localization. *J Neurophysiol* 32: 613–636, 1969. doi:10.1152/jn.1969.32.4.613.
6. **Yin TC**, **Chan JC.** Interaural time sensitivity in medial superior olive of cat. *J Neurophysiol* 64: 465–488, 1990. doi:10.1152/jn.1990.64.2.465.
7. **Pecka M**, **Brand A**, **Behrend O**, **Grothe B.** Interaural time difference processing in the mammalian medial superior olive: the role of glycinergic inhibition. *J Neurosci* 28: 6914–6925, 2008. doi:10.1523/JNEUROSCI.1660-08.2008.
8. **Roberts MT**, **Seeman SC**, **Golding NL.** A mechanistic understanding of the role of feedforward inhibition in the mammalian sound localization circuitry. *Neuron* 78: 923–935, 2013. doi:10.1016/j.neuron.2013.04.022.
9. **van der Heijden M**, **Lorteije JAM**, **Plauška A**, **Roberts MT**, **Golding NL**, **Borst JGG.** Directional hearing by linear summation of binaural inputs at the medial superior olive. *Neuron* 78: 936–948, 2013. doi:10.1016/j.neuron.2013.04.028.
10. **Myoga MH**, **Lehnert S**, **Leibold C**, **Felmy F**, **Grothe B.** Glycinergic inhibition tunes coincidence detection in the auditory brainstem. *Nat Commun* 5: 3790, 2014. doi:10.1038/ncomms4790.
11. **Franken TP**, **Roberts MT**, **Wei L**, **Golding NL**, **Joris PX.** In vivo coincidence detection in mammalian sound localization generates phase delays. *Nat Neurosci* 18: 444–452, 2015. doi:10.1038/nn.3948.
12. **Plauška A**, **M van der H**, **Borst JGG.** A test of the stereausis hypothesis for sound localization in mammals. *J Neurosci* 37: 7278–7289, 2017. doi:10.1523/JNEUROSCI.0233-17.2017.
13. **Ryan A.** Hearing sensitivity of the mongolian gerbil, *Meriones unguiculatis*. *J Acoust Soc Am* 59: 1222–1226, 1976. doi:10.1121/1.380961.
14. **Schmiedt RA.** Spontaneous rates, thresholds and tuning of auditory-nerve fibers in the gerbil: comparisons to cat data. *Hear Res* 42: 23–35, 1989. doi:10.1016/0378-5955(89)90115-9.
15. **Ohlemiller KK**, **Echteler SM.** Functional correlates of characteristic frequency in single cochlear nerve fibers of the Mongolian gerbil. *J Comp Physiol A* 167: 329–338, 1990. doi:10.1007/BF00192568.
16. **Schmiedt RA**, **Mills JH**, **Adams JC.** Tuning and suppression in auditory nerve fibers of aged gerbils raised in quiet or noise. *Hear Res* 45: 221–236, 1990. doi:10.1016/0378-5955(90)90122-6.
17. **Versteegh CPC**, **Meenderink SWF**, **Van der Heijden M.** Response characteristics in the apex of the gerbil cochlea studied through auditory nerve recordings. *J Assoc Res Otolaryngol* 12: 301–316, 2011. doi:10.1007/s10162-010-0255-y.
18. **Huet A**, **Batrel C**, **Tang Y**, **Desmadryl G**, **Wang J**, **Puel J-L**, **Bourien J.** Sound coding in the auditory nerve of gerbils. *Hear Res* 338: 32–39, 2016. doi:10.1016/j.heares.2016.05.006.
19. **Typlt M**, **Englitz B**, **Sonntag M**, **Dehmel S**, **Kopp-Scheinpflug C**, **Ruebsamen R.** Multidimensional characterization and differentiation of neurons in the anteroventral cochlear nucleus. *PLoS One* 7: e29965, 2012. doi:10.1371/journal.pone.0029965.
20. **Wei L**, **Karino S**, **Verschooten E**, **Joris PX.** Enhancement of phase-locking in rodents. I. An axonal recording study in gerbil. *J Neurophysiol* 118: 2009–2023, 2017. doi:10.1152/jn.00194.2016.
21. **Plauška A**, **Borst JG**, **van der Heijden M.** Predicting binaural responses from monaural responses in the gerbil medial superior olive. *J Neurophysiol* 115: 2950–2963, 2016. doi:10.1152/jn.01146.2015.
22. **Jurado C**, **Moore BCJ.** Frequency selectivity for frequencies below 100 Hz: comparisons with mid-frequencies. *J Acoust Soc Am* 128: 3585–3596, 2010. doi:10.1121/1.3504657.
23. **Brughera A**, **Dunai L**, **Hartmann W.** Human interaural time difference thresholds for sine tones: the high-frequency limit. *J Acoust Soc Am* 133: 2839–2855, 2013. doi:10.1121/1.4795778.
24. **Bernstein LR**, **Trahiotis C.** The normalized correlation: accounting for binaural detection across center frequency. *J Acoust Soc Am* 100: 3774–3784, 1996. doi:10.1121/1.417237.
25. **Raatgever J**, **Bilsen FA.** A central spectrum theory of binaural processing. Evidence from dichotic pitch. *J Acoust Soc Am* 80: 429–441, 1986. doi:10.1121/1.394039.
26. **Stern RM**, **Shear GD.** Lateralization and detection of low-frequency binaural stimuli: effects of distribution of internal delay. *J Acoust Soc Am* 100: 2278–2288, 1996. doi:10.1121/1.417937.
27. **Joris PX**, **van de Sande B**, **van der Heijden M.** Temporal damping in response to broadband noise. I. Inferior colliculus. *J Neurophysiol* 93: 1857–1870, 2005. doi:10.1152/jn.00962.2004.

Downloaded from journals.physiology.org/journal/jn (081.164.135.205) on July 13, 2026.

28. **Joris PX**, **Louage DH**, **van der Heijden M.** Temporal damping in response to broadband noise. II. Auditory nerve. *J Neurophysiol* 99: 1942–1952, 2008. doi:10.1152/jn.01179.2007.
29. **Stern RM**, **Zeiberg AS**, **Trahiotis C.** Lateralization of complex binaural stimuli: a weighted-image model. *J Acoust Soc Am* 84: 156–165, 1988 [Erratum in *J Acoust Soc Am* 90: 2202, 1991]. doi:10.1121/1.396982.
30. **Fay RR.** *Hearing in Vertebrates: A Psychophysics Databook*. Winnetka, IL: Hill-Fay Associates, 1988.
31. **Ruggero MA**, **Rich NC.** Chinchilla auditory-nerve responses to low-frequency tones. *J Acoust Soc Am* 73: 2096–2108, 1983. doi:10.1121/1.389577.
32. **Shofner WP**, **Sheft S**, **Guzman SJ.** Responses of ventral cochlear nucleus units in the chinchilla to amplitude modulation by low-frequency, two-tone complexes. *J Acoust Soc Am* 99: 3592–3605, 1996. doi:10.1121/1.414957.
33. **Ruggero MA**, **Narayan SS**, **Temchin AN**, **Recio A.** Mechanical bases of frequency tuning and neural excitation at the base of the cochlea: Comparison of basilar-membrane vibrations and auditory-nerve-fiber responses in chinchilla. *Proc Natl Acad Sci USA* 97: 11744–11750, 2000. doi:10.1073/pnas.97.22.11744.
34. **Recio-Spinoso A**, **Temchin AN**, **van Dijk P**, **Fan Y-H**, **Ruggero MA.** Wiener-kernel analysis of responses to noise of chinchilla auditory-nerve fibers. *J Neurophysiol* 93: 3615–3634, 2005. doi:10.1152/jn.00882.2004.
35. **Temchin AN**, **Rich NC**, **Ruggero MA.** Threshold tuning curves of chinchilla auditory-nerve fibers. I. Dependence on characteristic frequency and relation to the magnitudes of cochlear vibrations. *J Neurophysiol* 100: 2889–2898, 2008. doi:10.1152/jn.90637.2008.
36. **Temchin AN**, **Rich NC**, **Ruggero MA.** Threshold tuning curves of chinchilla auditory nerve fibers. II. Dependence on spontaneous activity and relation to cochlear nonlinearity. *J Neurophysiol* 100: 2899–2906, 2008. doi:10.1152/jn.90639.2008.
37. **Temchin AN**, **Ruggero MA.** Phase-locked responses to tones of chinchilla auditory nerve fibers: implications for apical cochlear mechanics. *J Assoc Res Otolaryngol* 11: 297–318, 2010. doi:10.1007/s10162-009-0197-4.
38. **Recio-Spinoso A.** Enhancement and distortion in the temporal representation of sounds in the ventral cochlear nucleus of chinchillas and cats. *PloS One* 7: e44286, 2012. doi:10.1371/journal.pone.0044286.
39. **Heinz MG**, **Swaminathan J.** Quantifying envelope and fine-structure coding in auditory nerve responses to chimaeric speech. *J Assoc Res Otolaryngol* 10: 407–423, 2009. doi:10.1007/s10162-009-0169-8.
40. **Heinz MG**, **Issa JB**, **Young ED.** Auditory-nerve rate responses are inconsistent with common hypotheses for the neural correlates of loudness recruitment. *J Assoc Res Otolaryngol* 6: 91–105, 2005. doi:10.1007/s10162-004-5043-0.
41. **Bremen P**, **Joris PX.** Axonal recordings from medial superior olive neurons obtained from the lateral lemniscus of the chinchilla (*Chinchilla laniger*). *J Neurosci* 33: 17506–17518, 2013. doi:10.1523/JNEUROSCI.1518-13.2013.
42. **Franken TP**, **Joris PX**, **Smith PH.** Principal cells of the brainstem's interaural sound level detector are temporal differentiators rather than integrators. *eLife* 7: e33854, 2018. doi:10.7554/eLife.33854.
43. **Joris PX**, **Carney LH**, **Smith PH**, **Yin TC.** Enhancement of neural synchronization in the anteroventral cochlear nucleus. I. Responses to tones at the characteristic frequency. *J Neurophysiol* 71: 1022–1036, 1994. doi:10.1152/jn.1994.71.3.1022.
44. **Joris PX**, **Smith PH**, **Yin TC.** Enhancement of neural synchronization in the anteroventral cochlear nucleus. II. Responses in the tuning curve tail. *J Neurophysiol* 71: 1037–1051, 1994. doi:10.1152/jn.1994.71.3.1037.
45. **Louage DHG**, **van der Heijden M**, **Joris PX.** Enhanced temporal response properties of anteroventral cochlear nucleus neurons to broadband noise. *J Neurosci* 25: 1560–1570, 2005. doi:10.1523/JNEUROSCI.4742-04.2005.
46. **van der Heijden M**, **Louage DHG**, **Joris PX.** Responses of auditory nerve and anteroventral cochlear nucleus fibers to broadband and narrowband noise: implications for the sensitivity to interaural delays. *J Assoc Res Otolaryngol* 12: 485–502, 2011. doi:10.1007/s10162-011-0268-1.
47. **Louage DHG**, **Joris PX**, **van der Heijden M.** Decorrelation sensitivity of auditory nerve and anteroventral cochlear nucleus fibers to broadband and narrowband noise. *J Neurosci* 26: 96–108, 2006. doi:10.1523/JNEUROSCI.2339-05.2006.
48. **Li Y-H**, **Joris PX.** Temporal correlates to monaural edge pitch in the distribution of interspike interval statistics in the auditory nerve. *eNeuro* 8: ENEURO.0292-21.2021, 2021. doi:10.1523/ENEURO.0292-21.2021.
49. **Joris PX.** Measuring ongoing delay with reverse noise. *J Acoust Soc Am* 151: A257, 2022. doi:10.1121/10.0011249.
50. **Perez-Flores MC**, **Verschooten E**, **Lee JH**, **Kim HJ**, **Joris PX**, **Yamoah EN.** Intrinsic mechanical sensitivity of mammalian auditory neurons as a contributor to sound-driven neural activity. *eLife* 11: e74948, 2022. doi:10.7554/eLife.74948.
51. **Pfeiffer RR.** Classification of response patterns of spike discharges for units in the cochlear nucleus: tone-burst stimulation. *Exp Brain Res* 1: 220–235, 1966. doi:10.1007/BF00234343.
52. **Godfrey DA**, **Kiang NY**, **Norris BE.** Single unit activity in the posteroventral cochlear nucleus of the cat. *J Comp Neurol* 162: 247–268, 1975. doi:10.1002/cne.901620206.
53. **Bourk TR.** Electrical Responses of Neural Units in the Anteroventral Cochlear Nucleus of the Cat (PhD thesis). Cambridge, MA: Massachusetts Institute of Technology, 1976.
54. **Rhode WS**, **Smith PH.** Encoding timing and intensity in the ventral cochlear nucleus of the cat. *J Neurophysiol* 56: 261–286, 1986. doi:10.1152/jn.1986.56.2.261.
55. **Blackburn CC**, **Sachs MB.** Classification of unit types in the anteroventral cochlear nucleus: PST histograms and regularity analysis. *J Neurophysiol* 62: 1303–1329, 1989. doi:10.1152/jn.1989.62.6.1303.
56. **Smith PH**, **Joris PX**, **Carney LH**, **Yin TC.** Projections of physiologically characterized globular bushy cell axons from the cochlear nucleus of the cat. *J Comp Neurol* 304: 387–407, 1991. doi:10.1002/cne.903040305.
57. **Smith PH**, **Joris PX**, **Yin TC.** Projections of physiologically characterized spherical bushy cell axons from the cochlear nucleus of the cat: evidence for delay lines to the medial superior olive. *J Comp Neurol* 331: 245–260, 1993. doi:10.1002/cne.903310208.
58. **Mardia KV**, **Jupp PE.** *Directional Statistics*. New York: John Wiley & Sons, 1999.
59. **Joris PX**, **Smith PH.** Temporal and binaural properties in dorsal cochlear nucleus and its output tract. *J Neurosci* 18: 10157–10170, 1998. doi:10.1523/JNEUROSCI.18-23-10157.1998.
60. **Stabler SE**, **Palmer AR**, **Winter IM.** Temporal and mean rate discharge patterns of single units in the dorsal cochlear nucleus of the anesthetized guinea pig. *J Neurophysiol* 76: 1667–1688, 1996. doi:10.1152/jn.1996.76.3.1667.
61. **Spirou GA**, **Brownell WE**, **Zidanic M.** Recordings from cat trapezoid body and HRP labeling of globular bushy cell axons. *J Neurophysiol* 63: 1169–1190, 1990. doi:10.1152/jn.1990.63.5.1169.
62. **Smith PH**, **Joris PX**, **Yin TCT.** Anatomy and physiology of principal cells of the medial nucleus of the trapezoid body (MNTB) of the cat. *J Neurophysiol* 79: 3127–3142, 1998. doi:10.1152/jn.1998.79.6.3127.
63. **Palmer AR**, **Winter IM**, **Darwin CJ.** The representation of steady-state vowel sounds in the temporal discharge patterns of the guinea pig cochlear nerve and primarylike cochlear nucleus neurons. *J Acoust Soc Am* 79: 100–113, 1986. doi:10.1121/1.393633.
64. **Ruggero MA**, **Rich NC**, **Shivapuja BG**, **Temchin AN.** Auditory-nerve responses to low-frequency tones: intensity dependence. *Audit Neurosci* 2: 159–185, 1996.
65. **Salvi RJ**, **Hamernik RP**, **Henderson D.** Response patterns of auditory nerve fibers during temporary threshold shift. *Hear Res* 10: 37–67, 1983. doi:10.1016/0378-5955(83)90017-5.
66. **Rosowski JJ**, **Ravicz ME**, **Songer JE.** Structures that contribute to middle-ear admittance in chinchilla. *J Comp Physiol A Neuroethol Sens Neural Behav Physiol* 192: 1287–1311, 2006. doi:10.1007/s00359-006-0159-9.
67. **Kuenzel T**, **Borst JGG**, **van der Heijden M.** Factors controlling the input–output relationship of spherical bushy cells in the gerbil cochlear nucleus. *J Neurosci* 31: 4260–4273, 2011. doi:10.1523/JNEUROSCI.5433-10.2011.
68. **Kuenzel T**, **Nerlich J**, **Wagner H**, **Rübsamen R**, **Milenkovic I.** Inhibitory properties underlying non-monotonic input-output relationship in low-frequency spherical bushy neurons of the gerbil. *Front Neural Circuits* 9: 14, 2015. doi:10.3389/fncir.2015.00014.
69. **Keine C**, **Rübsamen R.** Inhibition shapes acoustic responsiveness in spherical bushy cells. *J Neurosci* 35: 8579–8592, 2015. doi:10.1523/JNEUROSCI.0133-15.2015.

Downloaded from journals.physiology.org/journal/jn (081.164.135.205) on July 13, 2026.

70. **Brownell WE.** Organization of the cat trapezoid body and the discharge characteristics of its fibers. *Brain Res* 94: 413–433, 1975. doi:10.1016/0006-8993(75)90226-7.
71. **Smith PH**, **Joris PX**, **Banks MI**, **Yin TCT.** Responses of cochlear nucleus cells and projections of their axons. In: *The Mammalian Cochlear Nuclei*, edited by Merchán MA, Juiz JM, Godfrey DA, Mugnaini E**.** Boston, MA: Springer, 1993, p. 349–360.
72. **Moore BCJ.** The role of temporal fine structure processing in pitch perception, masking, and speech perception for normal-hearing and hearing-impaired people. *J Assoc Res Otolaryngol* 9: 399–406, 2008. doi:10.1007/s10162-008-0143-x.
73. **Oxenham AJ.** Revisiting place and temporal theories of pitch. *Acoust Sci Technol* 34: 388–396, 2013. doi:10.1250/ast.34.388.
74. **Heinz MG**, **Colburn HS**, **Carney LH.** Evaluating auditory performance limits: i. one-parameter discrimination using a computational model for the auditory nerve. *Neural Comput* 13: 2273–2316, 2001. doi:10.1162/089976601750541804.
75. **Lorenzi C**, **Gilbert G**, **Carn H**, **Garnier S**, **Moore BCJ.** Speech perception problems of the hearing impaired reflect inability to use temporal fine structure. *Proc Natl Acad Sci USA* 103: 18866–18869, 2006. doi:10.1073/pnas.0607364103.
76. **Verschooten E**, **Desloovere C**, **Joris PX.** High-resolution frequency tuning but not temporal coding in the human cochlea. *PLoS Biol* 16: e2005164, 2018. doi:10.1371/journal.pbio.2005164.
77. **Joris PX**, **Verschooten E.** On the limit of neural phase locking to fine structure in humans. *Adv Exp Med Biol* 787: 101–108, 2013. doi:10.1007/978-1-4614-1590-9_12.
78. **Rayleigh L.** XII. On our perception of sound direction. *Lond Edinb Dublin Philos Mag J Sci* 13: 214–232, 1907. doi:10.1080/14786440709463595.
79. **Licklider JCR**, **Webster JC**, **Hedlun JM.** On the frequency limits of binaural beats. *J Acoust Soc Am* 22: 468–473, 1950. doi:10.1121/1.1906629.
80. **Kuwada S**, **Yin TC**, **Wickesberg RE.** Response of cat inferior colliculus neurons to binaural beat stimuli: possible mechanisms for sound localization. *Science* 206: 586–588, 1979. doi:10.1126/science.493964.
81. **Shofner WP.** Comparative aspects of pitch perception. In: *Pitch*, New York: Springer, 2005, p. 56–98. doi:10.1007/0-387-28958-5_3.
82. **Bowen M**, **Terreros G**, **Moreno-Gómez FN**, **Ipinza M**, **Vicencio S**, **Robles L**, **Delano PH.** The olivocochlear reflex strength in awake chinchillas is relevant for behavioural performance during visual selective attention with auditory distractors. *Sci Rep* 10: 14894, 2020. doi:10.1038/s41598-020-71399-8.
83. **Kiang NY-S**, **Watanabe T**, **Thomas EC**, **Clark LF.** *Discharge Patterns of Single Fibers in the Cat's Auditory Nerve*. Cambridge, MA: MIT Press, 1966.
84. **Franken TP**, **Bremen P**, **Joris PX.** Coincidence detection in the medial superior olive: mechanistic implications of an analysis of input spiking patterns. *Front Neural Circuits* 8: 42, 2014. doi:10.3389/fncir.2014.00042.
85. **Köppl C.** Phase locking to high frequencies in the auditory nerve and cochlear nucleus magnocellularis of the barn owl, *Tyto alba*. *J Neurosci* 17: 3312–3321, 1997. doi:10.1523/JNEUROSCI.17-09-03312.1997.
86. **Mc Laughlin M**, **van der Heijden M**, **Joris PX.** How secure is in vivo synaptic transmission at the calyx of Held? *J Neurosci* 28: 10206–10219, 2008. doi:10.1523/JNEUROSCI.2735-08.2008.
87. **Carr CE**, **Boudreau RE.** Organization of the nucleus magnocellularis and the nucleus laminaris in the barn owl: encoding and measuring interaural time differences. *J Comp Neurol* 334: 337–355, 1993. doi:10.1002/cne.903340302.
88. **Couchman K**, **Grothe B**, **Felmy F.** Medial superior olivary neurons receive surprisingly few excitatory and inhibitory inputs with balanced strength and short-term dynamics. *J Neurosci* 30: 17111–17121, 2010. doi:10.1523/JNEUROSCI.1760-10.2010.
89. **Gjoni E**, **Aguet C**, **Sahlender DA**, **Knott G**, **Schneggenburger R.** Ultrastructural basis of strong unitary inhibition in a binaural neuron. *J Physiol* 596: 4969–4982, 2018. doi:10.1113/JP276015.
90. **Callan AR**, **Heß M**, **Felmy F**, **Leibold C.** Arrangement of excitatory synaptic inputs on dendrites of the medial superior olive. *J Neurosci* 41: 269–283, 2021. doi:10.1523/JNEUROSCI.1055-20.2020.
91. **Ashida G**, **Funabiki K**, **Carr CE.** Theoretical foundations of the sound analog membrane potential that underlies coincidence detection in the barn owl. *Front Comput Neurosci* 7: 151, 2013. doi:10.3389/fncom.2013.00151.
92. **Ashida G**, **Funabiki K**, **Carr CE.** Biophysical basis of the sound analog membrane potential that underlies coincidence detection in the barn owl. *Front Comput Neurosci* 7: 102, 2013. doi:10.3389/fncom.2013.00102.
93. **Rudnicki M**, **Hemmert W.** High entrainment constrains synaptic depression levels of an in vivo globular bushy cell model. *Front Comput Neurosci* 11: 16, 2017. doi:10.3389/fncom.2017.00016.
94. **Palmer AR**, **Kuwada S.** Binaural and spatial coding in the inferior colliculus. In: *The Inferior Colliculus*, edited by Winer JA, Schreiner CE. New York: Springer, 2005, p. 377–410.
95. **Palmer AR**, **Rees A**, **Caird D.** Interaural delay sensitivity to tones and broad band signals in the guinea-pig inferior colliculus. *Hear Res* 50: 71–86, 1990. doi:10.1016/0378-5955(90)90034-M.
96. **Kiang NY**, **Moxon EC.** Physiological considerations in artificial stimulation of the inner ear. *Ann Otol Rhinol Laryngol* 81: 714–730, 1972. doi:10.1177/000348947208100513.
97. **Kiang NYS.** Curious oddments of auditory-nerve studies. *Hear Res* 49: 1–16, 1990. doi:10.1016/0378-5955(90)90091-3.
98. **Heil P**, **Peterson AJ.** Nelson's notch in the rate-level functions of auditory-nerve fibers might be caused by PIEZO2-mediated reverse-polarity currents in hair cells. *Hear Res* 381: 107783, 2019. doi:10.1016/j.heares.2019.107783.
99. **Liberman MC**, **Kiang NY-S.** Single-neuron labeling and chronic cochlear pathology. IV. Stereocilia damage and alterations in rate- and phase-level functions. *Hear Res* 16: 75–90, 1984. doi:10.1016/0378-5955(84)90026-1.
100. **Cai Y**, **Geisler CD.** Temporal patterns of the responses of auditory-nerve fibers to low-frequency tones. *Hear Res* 96: 83–93, 1996. doi:10.1016/0378-5955(96)00033-0.
101. **Cao X-J**, **Shatadal S**, **Oertel D.** Voltage-sensitive conductances of bushy cells of the mammalian ventral cochlear nucleus. *J Neurophysiol* 97: 3961–3975, 2007. doi:10.1152/jn.00052.2007.
102. **Wang Y**, **Manis PB.** Temporal coding by cochlear nucleus bushy cells in dba/2j mice with early onset hearing loss. *J Assoc Res Otolaryngol* 7: 412–424, 2006. doi:10.1007/s10162-006-0052-9.
103. **Englitz B**, **Tolnai S**, **Typlt M**, **Jost J**, **Rubsamen R.** Reliability of synaptic transmission at the synapses of held in vivo under acoustic stimulation. *PLoS One* 4: e7014, 2009. doi:10.1371/journal.pone.0007014.
104. **Joris PX**, **Smith PH.** The volley theory and the spherical cell puzzle. *Neuroscience* 154: 65–76, 2008. doi:10.1016/j.neuroscience.2008.03.002.
105. **Smith PH**, **Massie A**, **Joris PX.** Acoustic stria: anatomy of physiologically characterized cells and their axonal projection patterns. *J Comp Neurol* 482: 349–371, 2005. doi:10.1002/cne.20407.
106. **Rhode WS**, **Oertel D**, **Smith PH.** Physiological response properties of cells labeled intracellularly with horseradish peroxidase in cat ventral cochlear nucleus. *J Comp Neurol* 213: 448–463, 1983. doi:10.1002/cne.902130408.
107. **Ostapoff EM**, **Feng JJ**, **Morest DK.** A physiological and structural study of neuron types in the cochlear nucleus. II. Neuron types and their structural correlation with response properties. *J Comp Neurol* 346: 19–42, 1994. doi:10.1002/cne.903460103.
108. **Lu H-W**, **Smith P**, **Joris P.** Evidence for two octopus cell subtypes: an in vivo single-cell recording and labeling study. *Assoc Res Otolaryngol Abs* 43: 554–555, 2020. https://aro.org/wp-content/uploads/2020/09/ARO-2020-Abstracts_1-21-20-Web.pdf.

Downloaded from journals.physiology.org/journal/jn (081.164.135.205) on July 13, 2026.